

Numerical simulations of buoyancy instabilities in galaxy cluster plasmas with cosmic rays and anisotropic thermal conduction

Y. Rasera and B. Chandran

Space Science Center, University of New Hampshire, Durham, NH 03824, USA

yann.rasera@obspm.fr

ABSTRACT

In clusters of galaxies, the specific entropy of intracluster plasma increases outwards. Nevertheless, a number of recent studies have shown that the intracluster medium is subject to buoyancy instabilities due to the effects of cosmic rays and anisotropic thermal conduction. In this paper, we present a new numerical algorithm for simulating such instabilities. This numerical method treats the cosmic rays as a fluid, accounts for the diffusion of heat and cosmic rays along magnetic field lines, and enforces the condition that the temperature and cosmic-ray pressure remain positive. We carry out several tests to ensure the accuracy of the code, including the detailed matching of analytic results for the eigenfunctions and growth rates of linear buoyancy instabilities. This numerical scheme will be useful for simulating convection driven by cosmic-ray buoyancy in galaxy cluster plasmas and may also be useful for other applications, including fusion plasmas, the interstellar medium, and supernovae remnants.

Subject headings: methods: numerical, conduction, diffusion, convection, MHD, plasmas, cosmic rays, instabilities, galaxies: clusters: general, cooling flows

1. Introduction

The hierarchical model of galaxy formation successfully predicts the evolution of baryons in the universe over a wide range of scales assuming that supernovae feedback is taken into account (Kauffmann et al. 1999; Somerville & Primack 1999; Cole et al. 2000; Hatton et al. 2003; Springel & Hernquist 2003; Rasera & Teyssier 2006). However, the baryon budget remains inaccurate in large scale structures (large galaxies, groups or clusters) where the total amount of cold gas and stars is overestimated. This overcooling problem is particularly critical for galaxy clusters, in which the cooling time near the center of a cluster is often

much shorter than a cluster’s age. In the absence of heating, one would expect cooling flows to form in these clusters, with large amounts of plasma cooling and flowing in towards the center. However, the star formation rate in cluster cores is typically 10-100 times lower than the predictions of the cooling-flow model (McNamara 2004), and line emission from plasma at temperatures lower than one third of the virial temperature of the cluster is weak (Peterson et al. 2003; McNamara 2004). The inconsistency between the cooling-flow model and these observations is known as the “cooling-flow problem”.

A promising hypothesis to solve this puzzle is heating by active galactic nuclei (AGN) in cluster cores. Two main arguments support this idea. First, AGN power is expected to be a decreasing function of the specific entropy at a cluster’s center and therefore tends naturally towards a self-regulated state in which heating balances cooling (Nulsen 2004; Boehringer et al. 2004). Second, almost all cooling core clusters possess active central radio sources (Eilek 2004). However, one important problem remains: how is AGN power transferred to the ambient plasma? Over the last decade, a number of numerical simulations have been carried out to answer this question. In the first simulations (Churazov et al. 2001; Quilis et al. 2001; Brüggén et al. 2002; Brüggén & Kaiser 2002), thermal energy was injected near the center of a 2D or 3D cluster-like hydrostatic profile. This resulted in hot and underdense bubbles, which then rose buoyantly. By agitating the surrounding medium, these bubbles were able to reduce the cooling while achieving some correspondence with the observations of X-ray cavities seen in roughly one-fourth of the clusters of the Chandra archive (Bîrzan et al. 2004). Subsequent simulations extended these earlier works to include new physical ingredients, such as viscosity (Ruszkowski et al. 2004a,b; Reynolds et al. 2005; Brüggén et al. 2005; Sijacki & Springel 2006). It was found that viscous dissipation contributed to the energy transfer, and that viscosity helped to prevent bubbles from breaking up. Other studies (Reynolds et al. 2001, 2002; Omma & Binney 2004; Omma et al. 2004; Cattaneo & Teyssier 2006; Heinz et al. 2006) injected not only thermal energy but also kinetic energy in subrelativistic bipolar jets. This approach also leads to cavities, but the dynamics are different than in the previous works because of the initial momentum of the bubbles and because the energy is deposited over a more narrow range of angles. In this context, the importance of turbulence, magnetohydrodynamics effects, and plasma transport processes has been underlined by Vernaleo & Reynolds (2006), who suggested that these ingredients could prevent the heating from being highly concentrated along the jet axis, as is the case for one-fluid pure-hydrodynamics simulations of jets in clusters that are initially at rest.

The above simulations treated the intracluster medium (ICM) as a single fluid. In single-fluid simulations, when AGN-heated plasma at temperature T_{hot} mixes with ambient intracluster plasma at temperature T_0 , the result is a Maxwellian plasma with a temperature

intermediate between T_0 and T_{hot} . Although this approach is valid in clusters if T_{hot} is not too large, it breaks down if the hot particles are relativistic or transrelativistic, because then Coulomb collisions do not have sufficient time to bring the hot particles into thermal equilibrium with the ambient intracluster plasma. If we focus on hot protons, the type of collision that brings such protons most rapidly into thermal equilibrium with the background plasma is collisions with background electrons. The time scale for thermal electrons to remove energy from a hot proton is Gould (1972),

$$\tau_\epsilon = \frac{(\gamma - 1)m_p m_e v_p c^2}{4\pi e^4 n_e} \left[\ln \left(\frac{2m_e c v_p p}{\hbar (4\pi e^2 n_e / m_e)^{1/2}} \right) - \frac{v_p^2}{2c^2} \right], \quad (1)$$

with n_e the electron density, γ the Lorentz factor, v_p the proton velocity, e and m_e the electron charge and mass, p and m_p the proton momentum and mass, and \hbar the reduced Planck constant.

For a typical proton energy of $E \simeq 1$ GeV (transrelativistic regime) and a typical cluster-core electrons density of $n_e = 0.01 \text{ cm}^{-3}$, the thermalization time scale is $\tau_\epsilon \simeq 7$ Gyr, which is much larger than the time for protons to escape the cluster core via diffusion or convection. In this case, the ICM is essentially a two-fluid system similar to the interstellar medium of the galaxy, with a thermal background plasma plus a population of high-energy particles (cosmic rays).

There are a few problems with treating a mix of cosmic rays and thermal plasma as a single Maxwellian fluid. One is that the single-fluid approximation to the temperature contains the cosmic-ray contribution to the energy density, and thus overestimates the actual temperature of the thermal plasma. If the cosmic-ray energy density is a significant fraction of the total energy density, the single-fluid model is unable to accurately predict the temperature profile of a cluster. In addition, since the thermal conductivity depends sensitively on the temperature ($\kappa_T \propto T^{5/2}$), and since conduction can make an important contribution to the heating of a cluster core (Zakamska & Narayan 2003) errors in the temperature profile can also lead to significant secondary errors in the thermal balance of the ICM.

A more subtle difficulty in applying a one-fluid model to a cosmic-ray/thermal-plasma mixture concerns the convective stability of intracluster plasma. It turns out that a radial gradient in the cosmic-ray energy density is much more destabilizing than a radial gradient in the thermal plasma energy density when the plasma mass density decreases outwards (see Eq.69 below). A correct accounting of the fraction of the total pressure contribution by cosmic rays is thus essential for understanding the convective stability of clusters. A more extensive discussion of this point is given by Chandran & Dennis (2006).

A more accurate treatment of the ICM, in which the cosmic rays are treated as either

a second fluid or as collisionless particles, is thus needed. In this paper, we present a new numerical algorithm for simulating the ICM that treats the ICM as a two-fluid (cosmic-ray plus thermal-plasma) system. We also present the results of a suite of tests for our code. Our numerical approach is similar to that of Mathews & Brighenti (2008), who carried out two-fluid simulations of cosmic-ray bubbles in the ICM. However, in contrast to this latter study, we take thermal conduction and cosmic-ray diffusion to occur almost entirely along magnetic field lines (cross-field transport arising only from numerical diffusion). Such anisotropic transport arises in clusters because the Coulomb mean free paths of thermal particles in clusters are much larger than their gyroradii, and the scattering mean free paths of cosmic rays are much larger than their gyroradii. The effects of magnetic fields on conduction are some times taken into account in when considering thermal conduction over length scales much larger than the correlation length of the (tangled) intracluster magnetic field, $l_B \simeq 1 - 10$ kpc (Kronberg 1994; Taylor et al. 2001, 2002; Vogt & Enßlin 2003). In this case, the conductivity κ_T is effectively isotropic (Rechester & Rosenbluth 1978; Chandran & Cowley 1998) with a value that is $\simeq 0.1 - 0.2$ times the Spitzer thermal conductivity for a non-magnetized plasma (Narayan & Medvedev 2001; Chandran & Maron 2004; Maron et al. 2004). However, on scales $\lesssim l_B$, the anisotropy of the thermal conductivity has a powerful effect on the convective stability of the intracluster medium (Balbus 2000, 2001; Parrish & Stone 2005; Chandran & Dennis 2006; Parrish & Stone 2007; Parrish & Quataert 2008; Quataert 2008), in such a way as to make convection much more likely than when the conductivity is treated as isotropic. This is true even if the magnetic field is so weak that the Lorentz force is negligible. In order to simulate buoyancy instabilities and convection in clusters, it is thus essential to incorporate anisotropic transport.

The remainder of this paper is organized as follows. In section 2 we present the basic equations of our two-fluid model. In section 3 we present the total-variation-diminishing (TVD) code that we use to solve these equations as well as several numerical tests, focusing on the case in which there is no conduction or diffusion. In section 4 we present the standard numerical discretization method for anisotropic conduction. We show how it can lead to negative temperature as emphasized before by Sharma & Hammett (2007). We then describe our new method that does not suffer from negative temperature problems. Tests such as the circular conduction test and Sovinec-test are also presented. Finally, in section 5 we present results for the linear buoyancy instabilities involving cosmic rays and anisotropic transport and compare our numerical solutions to analytic results.

2. Two-fluid equations with anisotropic transport

In order to carry-out realistic cluster simulations one has to deal with an impressive list of components (dark matter, plasma, cosmic rays, magnetic field, stars, supernovæ, supermassive black holes) and physical ingredients (advection, shocks, induction, gravity, anisotropic transport, cooling, energy injection from the AGN, feedback from supernovæ, jets, viscosity...). In this paper, rather than attempting to simulate all of these processes, we focus on developing an accurate and efficient numerical algorithm for simulating collisional plasmas pervaded by collisionless cosmic rays. A complete description of the cosmic rays in such a system would require us to solve for the cosmic-ray distribution function $f(\mathbf{r}, \mathbf{p}, t)$, where \mathbf{r} is the position coordinate, \mathbf{p} is momentum, and t is time. The resulting system of equations is much more difficult to solve numerically than a system of fluid equations because f depends on three momentum coordinates as well as position and time. However, in many situations of interest, f is nearly isotropic in momentum space and can be treated as function of only $(\mathbf{r}, |\mathbf{p}|, t)$ (Skilling 1975). Miniati (2001); Miniati et al. (2001) took advantage of this fact with a numerical code, COSMOCR, that solves for the evolution of f as a function of both \mathbf{r} and p . In this paper, we adopt the more simplistic and less computationally intensive fluid-like approach of Drury & Voelk (1981), which does not attempt to solve for the momentum dependence of f , but instead solves directly for the evolution of the cosmic-ray pressure p_{cr} as a function of \mathbf{r} and t . This model of Drury & Voelk (1981) has been extended to three spatial dimensions by Jones & Kang (1990), to include gravity by Mathews & Brighenti (2008), and to include the magnetic field and Lorentz force by Ryu et al. (2003). In this paper, we extend the model further to include anisotropic thermal conduction. The resulting equations can be written,

$$\frac{\partial \rho}{\partial t} + \nabla \cdot (\rho \mathbf{v}) = 0 \quad (2)$$

$$\frac{\partial \rho \mathbf{v}}{\partial t} + \nabla \cdot \left(\rho \mathbf{v} \mathbf{v} + p_{tot} \mathbf{I} - \frac{\mathbf{B} \mathbf{B}}{4\pi} \right) = \rho \mathbf{g} \quad (3)$$

$$\frac{\partial \mathbf{B}}{\partial t} - \nabla \times (\mathbf{v} \times \mathbf{B}) = 0 \quad (4)$$

$$\frac{\partial e}{\partial t} + \nabla \cdot \left((e + p_{tot}) \mathbf{v} - \frac{\mathbf{B}(\mathbf{B} \cdot \mathbf{v})}{4\pi} \right) = \rho \mathbf{v} \cdot \mathbf{g} + \nabla \cdot (\boldsymbol{\kappa} \cdot \nabla T) + \nabla \cdot (\mathbf{D} \cdot \nabla e_{cr}) \quad (5)$$

$$\frac{\partial e_{cr}}{\partial t} + \nabla \cdot (e_{cr} \mathbf{v}) = -p_{cr} \nabla \cdot \mathbf{v} + \nabla \cdot (\mathbf{D} \cdot \nabla e_{cr}), \quad (6)$$

with the 9 main variables, ρ the plasma density, $\rho \mathbf{v}$ the plasma momentum, \mathbf{B} the magnetic field, e_{cr} the cosmic ray internal energy, and $e = 0.5\rho v^2 + e_{th} + e_{cr} + 0.5B^2/4\pi$ the total energy. Intermediate variables are e_{th} , the internal thermal energy and $p_{tot} = (\gamma - 1)e_{th} +$

$(\gamma_{cr} - 1)e_{cr} + 0.5B^2/4\pi$ the total pressure with γ and γ_{cr} the adiabatic indices of gas and cosmic rays. \mathbf{g} is an external gravity field (the large scale gravitational potential is mostly dominated by stars and dark matter in galaxy clusters). Finally, \mathbf{D} and $\boldsymbol{\kappa}$ are the diffusion and conduction tensor, which are described further in section 4.

In this model, the cosmic rays flow at the same speed as the thermal plasma, since both are frozen to the same magnetic field lines and since wave-particle interactions limit the relative motion between cosmic rays and thermal plasma in the direction of the magnetic field. On the other hand, because the pitch-angle scattering associated with wave-particle interactions is of finite strength, the cosmic rays can diffuse with respect to the thermal plasma. We have taken this diffusion, as well as the conduction of heat, to occur entirely along magnetic field lines. This is a reasonable approximation in clusters of galaxies, because the gyroradii of thermal particles are much shorter than their collisional mean free paths, and the gyroradii of cosmic rays are much shorter than their scattering mean free paths. The value of the cosmic-ray diffusion coefficient in clusters of galaxies is not well known. In this paper, we use a value $D_{\parallel} = 10^{29} \text{ cm}^2\text{s}^{-1}$ comparable to the parallel diffusion coefficient of 1 GeV protons in the interstellar medium of our galaxy.

We assume that protons dominate the cosmic-ray energy density in clusters, as is the case in the Galaxy. For protons in clusters, the energy loss times associated with Coulomb interactions and inelastic collisions (pion production) are typically longer than the growth times of the instabilities that we focus on in this paper. Thus, we neglect Coulomb losses and pion production in this paper. We note that we also do not include self-gravity, since it is not important in the hot intracluster medium.

It can be seen from equation 6 that the cosmic rays are treated as a fluid with adiabatic index γ_{cr} . Thus, if $\nabla \cdot \mathbf{v} < 0$ at some location, the converging flow acts to increase the cosmic-ray pressure. If we were to model the cosmic-ray distribution function $f(\mathbf{r}, \mathbf{p}, t)$ as a power law in momentum of the form $p^2 f \propto p^{-\alpha}$ with a low energy cutoff, then the effective value of γ_{cr} is given by equation [13] of Jubelgas et al. (2008). In this paper we make the simple choice that

$$\gamma_{cr} = 4/3, \tag{7}$$

corresponding to the limit in which α approaches 2 from above, and in which the cosmic-ray energy density is dominated by ultra-relativistic particles.

We note that our approach is in some ways similar to the model of Jubelgas et al. (2008), who incorporated cosmic rays into hydrodynamical simulations of galaxy formation based on smoothed particle hydrodynamics. Their approach, like ours, employs an effective adiabatic index for the cosmic rays and avoids solving for the full cosmic-ray momentum distribution function. However, Jubelgas et al. (2008) also develop a framework for incorporating a

number of effects that are not treated here, including ionization losses, radiation losses, and shock acceleration. On the other hand, Jubelgas et al. (2008) assume an isotropic cosmic-ray diffusion coefficient, whereas anisotropic transport of both cosmic rays and heat plays a central role in our model as well as the buoyancy instabilities that we simulate in section 5.3.

3. Numerical implementation and tests in the absence of transport

In this section, we set $\kappa = \mathbf{D} = \mathbf{0}$. Our numerical method for solving the magnetohydrodynamic-like (MHD-like) two-fluid equations is based on the Total Variation Diminishing (TVD) MHD code of Pen et al. (2003) which has the advantage of being fast, simple and efficient. This TVD MHD code is fully described in 3 papers. The appendix of Pen (1998) presents the relaxed TVD method that is used, Trac & Pen (2003) shows the different methods for hydrodynamics solver and Pen et al. (2003) describes the MHD code itself. We will here recall the main characteristics of this code but the reader should refer to the above articles for more complete explanations.

The fluid solver is a conservative, second-order (in space and time), dimensionally split, TVD, upwind scheme. In this relaxing TVD method, each hyperbolic conservation law is replaced by a left and a right advection problem with an advection speed called the “freezing speed”. By taking this freezing speed equals to the largest eigenvalue of the system $c = \max(|v| + c_s)$ (with c_s the sound speed and v the velocity along the updated direction), it ensures the scheme to be TVD. The advection problem is then solved using Van-Leer slope limiter to reach second order in space and Runge-Kutta integration to reach second order in time.

The magnetic field is updated separately in advection-constraints step. A staggered grid is used with \mathbf{B} defined on cell surfaces (see Fig.1) in order to satisfy the divergence-free magnetic field condition at machine precision. The advection step is computed using the same TVD method as in the fluid solver. This is however easier since the velocity is assumed to be fixed (operator splitting). The second order flux is then directly re-used to compute the constraint step. Here again Runge-Kutta is used for second order temporal accuracy.

This method is very efficient because it doesn’t need to solve the whole Riemann problem and therefore compute all eigenvalues. It only needs the computation of the largest one for the freezing speed. The resolution of slow waves is slightly degraded, however the code could still resolve shocks using only a few cells.

The fluid solver has successfully been tested for advection of a square wave and evolution of a three dimensionnal Sedov blast wave. Finally, the MHD code gives good results on

various tests such as slow, fast and Alfvén waves as well as an MHD shock-tube problem.

To modify this TVD code to solve equations (2) through (6), we include an additional fluid variable e_{cr} and use exactly the same routine. The flux vector associated with the conservative variables becomes (for an update along 'x'),

$$\mathbf{F} = \begin{pmatrix} \rho v_x \\ \rho v_x^2 + p + 0.5B^2/4\pi + p_{cr} - B_x^2/4\pi \\ \rho v_x v_y - B_x B_y/4\pi \\ \rho v_x v_z - B_x B_z/4\pi \\ (e_{tot} + p + 0.5B^2/4\pi + p_{cr})v_x - B_x \mathbf{B} \cdot \mathbf{v} \\ e_{cr} v_x \end{pmatrix},$$

with $p_{cr} = (\gamma_{cr} - 1)e_{cr}$. The freezing speed becomes $c = \max[|v_x| + \sqrt{(\gamma p + \gamma_{cr} p_{cr} + B^2/4\pi)/\rho}]$ and the timestep is reduced to $dt = 0.8\Delta x / \max[|v_x|, |v_y|, |v_z|] + \sqrt{(\gamma p + \gamma_{cr} p_{cr} + B^2/4\pi)/\rho}$. In this way, we recover the original MHD TVD method when $p_{cr} = 0$ and otherwise take into account effects of cosmic rays using the same TVD routine.

The remaining source term $-p_{cr} \nabla \cdot \mathbf{v}$ is related to the pressure work during expansion or contraction and is easy to implement. Following the general philosophy of the code, we discretize it at second order accuracy using dimensional splitting for multidimensional runs and Runge-Kutta to reach second order temporal accuracy. It leads to:

$$-p_{cr}^n \frac{v_{i+1}^n - v_{i-1}^n}{2\Delta x}. \quad (8)$$

This contribution is finally included in the energy update at the beginning of each one-dimensional hydrodynamics step. In the following sections, we describe several tests of this 2-fluids code that we have performed.

3.1. Linear test: propagation of a sound wave in a composite of cosmic rays and thermal gas

The first simple test is the propagation of sound wave in a medium with cosmic rays and plasma. The adiabatic wave speed is given by

$$c_s = \sqrt{\frac{\gamma p_0 + \gamma_{cr} p_{cr0}}{\rho_0}}, \quad (9)$$

with ρ_0 , p_0 and p_{cr0} the initial non-perturbed quantities. In order to trigger an eigenfunction, we need to satisfy the following relations between the field perturbations,

$$\frac{\delta \rho}{\rho_0} = \frac{\delta v}{c_s}, \quad (10)$$

$$\frac{\delta p}{p_0} = \gamma \frac{\delta v}{c_s}, \quad (11)$$

$$\frac{\delta p_{cr}}{p_{cr0}} = \gamma_{cr} \frac{\delta v}{c_s}, \quad (12)$$

with δv , $\delta \rho$, δp and δp_{cr} the perturbations. For our test, we take for the equilibrium quantities $v_0 = 0$, $\rho_0 = 1$, $p_0 = 1$ and $p_{cr0} = 1$. We then perturbate the velocity with a sine of amplitude $\delta v = 10^{-3}$ and wavelength 0.5. The other quantities are perturbed following 10, 11 and 12.

Fig.2 shows the results after a propagation during one period for 128 grid points. The result is in good agreement with the analytical solution and we obtain the same level of accuracy achieved in a pure hydrodynamical simulation (without cosmic rays). The slight smoothing of the extrema is due to the slope limiter which prevents the code from introducing spurious oscillations.

3.2. Non Linear test: Riemann shock-tube problem for a composite of cosmic rays and thermal gas

A more challenging test is the Riemann shock-tube problem. The standard problem (Sod 1978; Hawley et al. 1984) involves a polytropic gas starting with a state of high pressure and high density in the half-left space and a state of low density and low pressure in the half-right space. It leads to 5 regions with different fluid states separated by the head and tail of the rarefaction wave, the contact discontinuity and the shock. The interesting point is that one can derive the analytical solution using the Rankine-Hugoniot conditions.

However, in our case the composite of cosmic rays and thermal gas is not a polytropic fluid and this solution doesn't apply. This problem has been solved by Pfrommer et al. (2006) and we use here their analytical solution. Our 1D initial conditions are close to the ones used in their article with a left-hand state (L) and a right-hand state (R) in the simulation box. They are given (using an appropriate system of units) by,

$$1 < x < 1.5 \quad 1.5 \leq x < 2, \quad (13)$$

$$\rho_L = 1 \quad \rho_R = 0.2, \quad (14)$$

$$v_L = 0 \quad v_R = 0, \quad (15)$$

$$p_L = 6.7 \times 10^4 \quad p_R = 2.4 \times 10^2, \quad (16)$$

$$p_{crL} = 1.3 \times 10^5 \quad p_{crR} = 2.4 \times 10^2. \quad (17)$$

$$(18)$$

The sound speed is therefore $c_{sL} = 537$ and $c_{sR} = 60$. We run a simulation with 1024 grid points until $t = 4.4 \times 10^{-4}$ so that the shock front has propagated on an important fraction of the box length $L = 1$.

Here again, there is a good agreement between the simulation results and the analytical prediction (see Fig.3). The transitions between the 5 states are well situated. The shock is resolved using few cells. As in Pen et al. (2003) some variables have a slight overshoot in the first postshock cell but this doesn't affect the other subsequent cells. The contact discontinuity is slightly smoothed by the relaxation solver. To conclude, the accuracy is similar to the accuracy obtained in the 1-fluid shock tube test and the implementation of cosmic rays is successful.

4. Anisotropic transport: heat conduction and cosmic-ray diffusion

In the presence of a magnetic field, the heat conduction in a plasma takes the form

$$\frac{\partial e}{\partial t} = \nabla \cdot (\kappa_{\parallel} \hat{\mathbf{b}} \hat{\mathbf{b}} \cdot \nabla T) + \nabla \cdot [\kappa_{\perp} (\mathbf{I} - \hat{\mathbf{b}} \hat{\mathbf{b}}) \nabla T], \quad (19)$$

with κ_{\perp} the perpendicular conductivity and κ_{\parallel} the parallel conductivity and $\hat{\mathbf{b}}$ the unit vector along the magnetic field (Braginskii 1965). We will focus here on this equation, but one has to keep in mind that the diffusion of cosmic rays has a similar form

$$\frac{\partial e_{cr}}{\partial t} = \nabla \cdot (D_{\parallel} \hat{\mathbf{b}} \hat{\mathbf{b}} \cdot \nabla e_{cr}) + \nabla \cdot [D_{\perp} (\mathbf{I} - \hat{\mathbf{b}} \hat{\mathbf{b}}) \nabla e_{cr}], \quad (20)$$

with D_{\perp} the perpendicular diffusion coefficient and D_{\parallel} the parallel diffusion coefficient. This equation is therefore solved by the same subroutine.

In cluster of galaxies the ion giroradius is much smaller than the mean free path between particle collisions and therefore the perpendicular part could be neglected since $\kappa_{\perp} \ll \kappa_{\parallel}$ (and $D_{\perp} \ll D_{\parallel}$ for cosmic rays). The conduction is highly anisotropic, primarily along the magnetic field, and mainly due to electrons. We adopt here the Spitzer value κ_s for the conductivity (Spitzer 1962) of an ionised plasma with the Coulomb logarithm $\ln \lambda$ set to a typical value for clusters:

$$\kappa_{\parallel} = \kappa_S = 9.2 \times 10^{30} n_e k_B \left(\frac{k_B T}{5 \text{ keV}} \right)^{\frac{5}{2}} \left(\frac{n_e}{0.01 \text{ cm}^{-3}} \right)^{-1} \left(\frac{37}{\ln \lambda} \right) \text{ cm}^2 \cdot \text{s}^{-1} \quad (21)$$

For the parallel diffusion coefficient of the cosmic rays, we set

$$D_{\parallel} = 10^{29} \text{ cm}^2 \cdot \text{s}^{-1}. \quad (22)$$

4.1. Implementation and tests

4.1.1. Centered asymmetric method: advantages and drawbacks

The first method we implemented uses the so-called centered asymmetric differencing. It is the most natural conservative discretization and it has been shown to give good results by Parrish & Stone (2005, 2007). The idea is to compute the heat flux F on each face and then to evolve the energy using an explicit time integration. We will consider only two dimensions but the generalisation to three dimensions is straightforward. The update of the energy is,

$$-\frac{e_{i,j}^{n+1} - e_{i,j}^n}{\Delta t} = \frac{F_{i+1/2,j}^n - F_{i-1/2,j}^n}{\Delta x} + \frac{F_{i,j+1/2}^n - F_{i,j-1/2}^n}{\Delta y}. \quad (23)$$

This is the starting point for any conservative methods, now the problem is to evaluate the face-centered flux. The flux at time n and position $(i + 1/2, j)$ is given by (see Fig.4),

$$F_{i+1/2,j}^n = b_x \bar{\kappa}_{\parallel} (b_x \frac{\partial T}{\partial x} + \bar{b}_y \frac{\partial T}{\partial y}), \quad (24)$$

$$b_x = b_{x,i+1/2,j}^n, \quad (25)$$

$$\bar{\kappa}_{\parallel} = \frac{\kappa_{i,j} + \kappa_{i+1,j}}{2}, \quad (26)$$

$$\frac{\partial T}{\partial x} = \frac{T_{i+1,j} - T_{i,j}}{\Delta x}, \quad (27)$$

$$\bar{b}_y = \frac{b_{y,i,j-1/2} + b_{y,i,j+1/2} + b_{y,i+1,j-1/2} + b_{y,i+1,j+1/2}}{4} \quad (28)$$

$$\frac{\partial T}{\partial y} = \frac{T_{i+1,j+1} - T_{i+1,j-1} + T_{i,j+1} - T_{i,j-1}}{4\Delta y}. \quad (29)$$

The x component of the temperature gradient and the magnetic field are well known in $(i + 1/2, j)$, however the y components need to be extrapolated (overline). The time step is chosen to ensure linear stability

$$\Delta t = 0.45 \min \left(\frac{\Delta x^2}{2D_{\text{cond}}} \right), \quad (30)$$

$$D_{\text{cond}} = (\gamma - 1) \frac{\kappa_{\parallel}}{\rho} \frac{\mu m_H}{k_B}. \quad (31)$$

This method is fast, efficient and accurate. However, as highlighted by Sharma & Hammett (2007), this method is *not positive definite*. Indeed, it could lead to negative temperature in presence of large temperature gradient. An easy way to see the problem is to notice that in the flux expression $T_{i+1,j+1}$ and $T_{i,j+1}$ appear with positive signs. So if one of this

temperature is a lot larger than all the others then nothing could balance this very large negative contribution and the energy $e_{i,j}^{n+1}$ could become negative. This problem is due to the spatial discretization itself and not to the explicit scheme used for time integration. The transverse temperature gradient is not computed from the same origin as where the energy is taken, this is the heart of the problem. An implicit scheme (Sovinec et al. 2005; Balsara et al. 2008) could therefore also suffer from the same negative temperature issues. One could indeed imagine the same situation as before but where the very large temperature $T_{i+1,j-1}$ or $T_{i,j-1}$ stays relatively constant until the time step t^{n+1} . Then, the energy $e_{i,j}^{n+1}$ could also become negative with an implicit scheme.

There are two methods to make the scheme positive: the first one consists in limiting the transverse gradient $\frac{\partial T}{\partial y}$. This idea is described in full detail in Sharma & Hammett (2007). The second one consists in another discretization of the problem and is described in the following section.

4.1.2. Positive anisotropic heat conduction: the flux-tube method

We present here a new positive method for anisotropic conduction. It is based on a physically motivated discretization which treats anisotropic conduction as a 1D diffusion process along the field lines. One could indeed simplify the discretization by considering only one thin magnetic flux-tube containing (i, j) and by calculating the temperature gradient and energy flux directly along this flux tube. Using $\nabla \cdot \mathbf{B} = 0$, the anisotropic conduction equation

$$\frac{\partial e}{\partial t} = \nabla \cdot \left(\frac{\mathbf{B}}{B} \kappa_{\parallel} \hat{\mathbf{b}} \cdot \nabla T \right) \quad (32)$$

could be rewritten as

$$\frac{\partial e}{\partial t} = \mathbf{B} \cdot \nabla \left(\frac{\kappa_{\parallel}}{B} \hat{\mathbf{b}} \cdot \nabla T \right), \quad (33)$$

or,

$$\frac{1}{B} \frac{\partial e}{\partial t} = \hat{\mathbf{b}} \cdot \nabla \left(\frac{\kappa_{\parallel}}{B} \hat{\mathbf{b}} \cdot \nabla T \right), \quad (34)$$

where $\hat{\mathbf{b}} = \mathbf{B}/B$. One can see the apparition of the derivative along the magnetic field, and the term $1/B$ to satisfy magnetic flux conservation. Because $B \cdot A = \text{constant}$, where A is the cross-section area of a flux-tube, the $1/B$ term can be thought of as representing the cross-sectional area A .

We now define s as the curvilinear abscissa along the field lines. The origin of this curvilinear abscissa is chosen to be $s = 0$ at the grid point (i, j) of interest. In order to compute derivatives, we consider variations over a length $\Delta s = \Delta x$ along the field line. The derivative of a function f_s in (i, j) becomes $(f_{+\Delta s/2} - f_{-\Delta s/2})/\Delta s$ and the same function derived in $+\Delta s/2$ gives $(f_{+\Delta s} - f_0)/\Delta s$.

The discretization along the flux-tube is therefore (see Fig.5),

$$\frac{e_0^{n+1} - e_0^n}{\Delta t} = \frac{B_0}{\Delta s} \left[\left(\frac{\kappa_{\parallel}}{B} \frac{\partial T}{\partial s} \right)_{+\Delta s/2} - \left(\frac{\kappa_{\parallel}}{B} \frac{\partial T}{\partial s} \right)_{-\Delta s/2} \right], \quad (35)$$

$$\left(\frac{\partial T}{\partial s} \right)_{+\Delta s/2} = \frac{\bar{T}_{+\Delta s} - T_0}{\Delta s}, \quad (36)$$

$$\left(\frac{\partial T}{\partial s} \right)_{-\Delta s/2} = \frac{T_0 - \bar{T}_{-\Delta s}}{\Delta s}, \quad (37)$$

$$\kappa_{\parallel, -\Delta s/2} = \frac{\bar{\kappa}_{\parallel, -\Delta s} + \kappa_{\parallel, 0}}{2}, \quad (38)$$

$$\kappa_{\parallel, +\Delta s/2} = \frac{\bar{\kappa}_{\parallel, +\Delta s} + \kappa_{\parallel, 0}}{2}, \quad (39)$$

$$B_{-\Delta s/2} = \frac{\bar{B}_{-\Delta s} + B_0}{2}, \quad (40)$$

$$B_{+\Delta s/2} = \frac{\bar{B}_{+\Delta s} + B_0}{2}, \quad (41)$$

with the subscript indicating the curvilinear abscissa where the value is computed and the overline meaning that the value is not directly known and has therefore to be interpolated from grid point values.

The next step is to estimate the position $\mathbf{X}(s)$ corresponding to $s = \pm\Delta s$ in the cartesian grid, which is done at second order,

$$\mathbf{X}(s) = \hat{\mathbf{b}}_0 s + 0.5s^2(\hat{\mathbf{b}}_0 \cdot \nabla)\hat{\mathbf{b}}_0, \quad (42)$$

$$(\hat{\mathbf{b}}_0 \cdot \nabla)\hat{\mathbf{b}}_{x,0} = b_{x,i,j} \frac{b_{x,i+1,j} - b_{x,i-1,j}}{2\Delta x} + b_{y,i,j} \frac{b_{x,i,j+1} - b_{x,i,j-1}}{2\Delta x}, \quad (43)$$

$$(\hat{\mathbf{b}}_0 \cdot \nabla)\hat{\mathbf{b}}_{y,0} = b_{x,i,j} \frac{b_{y,i+1,j} - b_{y,i-1,j}}{2\Delta x} + b_{y,i,j} \frac{b_{y,i,j+1} - b_{y,i,j-1}}{2\Delta x}. \quad (44)$$

The final and fundamental step is the interpolation of the temperature at the curvilinear abscissa $s = \pm\Delta s$. This will determine the accuracy of the method, as well as the positivity of the scheme. For this purpose, we decompose the 2D interpolation into a series of 1D interpolations that are done with the second-order Lagrange interpolating formula. An important point, is that whatever the position we consider, we only interpolate using

(i, j) and the 8 surrounding points. This is more convenient for the boundary conditions. Unfortunately, second-order interpolations are not guaranteed to stay in the range defined by the 2 extrema of the 9 considered point. Allowing such overshoot could create oscillations and negative temperature. We therefore saturate the interpolation to the extrema of the 9 considered point, in order to allow positivity of the scheme. One drawback is that we loose accuracy near extrema, but this is unavoidable in order to get physical results. We will also see that the resulting amount of artificial diffusion is small. Finally, the norm of the magnetic field and the conductivity are interpolated only at first order for speed and therefore don't need to be saturated. One could interpolate at higher order for better accuracy.

It is interesting to note that one could rewrite the update of the energy as,

$$T_0^{n+1} = T_0^n + \alpha \left(\frac{A_{-\Delta s/2} T_{-\Delta s} + A_{+\Delta s/2} T_{+\Delta s}}{A_{-\Delta s/2} + A_{+\Delta s/2}} - T_0^n \right), \quad (45)$$

$$A_{-\Delta s/2} = \frac{\kappa_{\parallel, -\Delta s/2}}{\kappa_{\parallel, 0}} \frac{B_0}{B_{-\Delta s/2}}, \quad (46)$$

$$A_{+\Delta s/2} = \frac{\kappa_{\parallel, +\Delta s/2}}{\kappa_{\parallel, 0}} \frac{B_0}{B_{+\Delta s/2}}, \quad (47)$$

$$\alpha = D_{\text{cond}, 0} \frac{\Delta t}{\Delta s^2} (A_{-\Delta s/2} + A_{+\Delta s/2}), \quad (48)$$

$$D_{\text{cond}, 0} = \kappa_{\parallel, 0} \frac{\gamma - 1}{\rho_0} \frac{\mu m_H}{k_B}. \quad (49)$$

It means that the temperature T_0 evolve by a fraction α toward the arithmetic average of $T_{-\Delta s}$ and $T_{+\Delta s}$. We therefore choose the time step like in the precedent method that is to say, $\Delta t = 0.45 \text{ min} (\Delta x^2 / (2D_{\text{cond}}))$. Using this time step and computing the norm of the magnetic field by 40 and 41, it guarantees that $\alpha \leq 1$ and prevents from any overshoot of the average. Since the interpolated temperature $T_{-\Delta s}$ and $T_{+\Delta s}$ are between the extrema of the neighbors of T_0 , it means that no oscillations could appear! We have therefore implemented a positive flux-tube scheme for anisotropic conduction and diffusion.

4.1.3. Diffusion of a step function

The first test we run is the passive diffusion of a 1D Heavyside function. The goal here is to check if the code solves well the diffusion along straight magnetic field lines. In a second test we will check how well the code follows curved magnetic field line. We start here with the following conditions,

$$\rho = 1, b = 1 \quad \text{everywhere} \quad (50)$$

$$e = 1 \quad \text{for} \quad x \leq 0.5 \quad (51)$$

$$e = 2 \quad \text{for} \quad 0.5 < x \leq 0.75 \quad (52)$$

$$e = 1 \quad \text{for} \quad x > 0.5 \quad (53)$$

We then use a constant conduction coefficient, $D_{\text{cond}} = 1$ so that the solution is analytically tractable. Our 100 grid points simulation is ran until $t = 2.8 \times 10^{-3}$. For one step of size Δe and mean e_0 situated at the location x_0 the analytical solution gives,

$$e(x, t) = e_0 + \frac{\Delta e}{2} \text{erf} \left(\frac{x - x_0}{\sqrt{4D_{\text{cond}}t}} \right). \quad (54)$$

The comparison in Fig.6 shows a very good agreement between the simulation and the analytical solution since we cannot differentiate them.

4.1.4. Anisotropic conduction in circular magnetic field lines

A more challenging test involves passive anisotropic diffusion along circular field lines, as proposed in Parrish & Stone (2005). The idea is to consider an initial hot patch embedded in circular magnetic field lines. The heat should then diffuse along the field lines but not across the field. We start here with the following initial condition:

$$\rho = 1 \quad \text{for} \quad 0 \leq x \leq 1 \text{ and } 0 \leq y \leq 1, \quad (55)$$

$$b_x = \frac{y - 0.5}{r} \quad \text{for} \quad 0 \leq x \leq 1 \text{ and } 0 \leq y \leq 1, \quad (56)$$

$$b_y = -\frac{x - 0.5}{r} \quad \text{for} \quad 0 \leq x \leq 1 \text{ and } 0 \leq y \leq 1, \quad (57)$$

$$e = 10000 \quad \text{for} \quad 0.7 \leq x \leq 0.8 \text{ and } 0.49 \leq y \leq 0.51, \quad (58)$$

$$e = 1 \quad \text{otherwise}, \quad (59)$$

with $r = \sqrt{(x - 0.5)^2 + (y - 0.5)^2}$.

The 100 by 100 simulation is run with $D_{\text{cond}} = 1$ using our flux-tube method as well as the standard centered asymmetric method. We also run the Van-Leer-limited implementation of Sharma & Hammett (2007). We present in Fig.7 the temperature profiles at $t = 0$, $t = 0.0225$, $t = 0.0675$ and $t = 0.18$ for these three methods.

In all three methods, the heat flux follows the circular field lines and tends toward a stationary solution without any angular gradient of temperature. When there is no perpendicular conductivity, the analytical stationary solution is obtained by energy conservation:

$e_{stat} = 128.3$ everywhere inside the shell. However, second order truncation errors add some artificial perpendicular diffusion. As a consequence the radial profile which was initially a Heavyside (as in the preceding test) diffuses. The consequence is that the maximum is lowered and the radial profile is smoothed.

If one uses the standard asymmetric differencing, the dramatic consequence is that it leads to negative temperatures, even after a long run time. These negative temperatures are shown as a white inner and outer circle with dotted contours in Fig.7, left column. This is a very important problem. On the numerical point of view, it indicates that this scheme could overshoot the extrema and therefore create some spurious oscillations. On the physical point of view, it means that heat can flow from lower to higher temperature. Moreover, while coupling with the MHD solver, it could lead to negative temperatures, create an imaginary sound speed, and lead to unphysical results.

All these points have been discussed in detail in Sharma & Hammett (2007). They found that this problem arises in presence of strong temperature gradient perpendicular to the magnetic field. This is why they proposed a limited version of this asymmetric discretisation, in which they limit the perpendicular temperature gradient. However, as they already mentioned, the perpendicular diffusion becomes important if one uses limited methods. This is obvious, in Fig.7, middle column. For example, in the last line, one could see that the radial dispersion is larger than in the asymmetric method. Moreover, the maximum has been decreased by a factor of 1.5.

On the contrary, our method combines two advantages of the two other methods. As presented in the right-hand column of Fig.7, the temperature always stays between the initial extrema but keep a low level of perpendicular diffusion. We are now going to estimate this perpendicular numerical diffusion using a test especially dedicated for this purpose.

4.1.5. Accuracy of the method: Sovinec test

In order to compare the accuracy of different methods, it is interesting to know what is the artificial perpendicular diffusivity of a scheme. Indeed, some applications could require a large ratio of the parallel to perpendicular conductivity. Sovinec et al. (2005) have developed such a test. We will therefore run this test for our method and compare our perpendicular artificial diffusion with the Van-Leer-limited method presented in Sharma & Hammett (2007) as well as the standard asymmetric method.

The idea is to consider the full heat equation 19 in 2D with both a perpendicular and an anisotropic part. We also add in this energy equation a heating source term $Q(x, y) =$

$Q_0 \times \cos(kx)\cos(ky)$. The equation to solve becomes,

$$\frac{\partial e}{\partial t} = \nabla \cdot \kappa_{\parallel} \hat{\mathbf{b}} \hat{\mathbf{b}} \cdot \nabla T + \nabla \cdot \left[\kappa_{\perp} (\mathbf{I} - \hat{\mathbf{b}} \hat{\mathbf{b}}) \nabla T \right] + Q(x, y). \quad (60)$$

The analytical stationary solution could be computed in the case of pure isotropic conduction ($\kappa_{\parallel} = \kappa_{\perp}$) with a constant conductivity. It is given by

$$T(x, y) = \frac{Q_0}{2\kappa_{\perp} k^2} \cos(kx)\cos(ky). \quad (61)$$

As in Sovinec et al. (2005), we consider a fixed magnetic field satisfying $\mathbf{B} \cdot \nabla T = 0$, so that the previous solution still apply. Taking into account artificial diffusion, the solution in the center becomes $T(0, 0) = Q_0 / [2k^2(\kappa_{\perp} + \kappa_{num})]$. The artificial diffusion could therefore easily be deduced from the central temperature.

Our initial conditions for $0.5 \leq x \leq 0.5$ and $0.5 \leq y \leq 0.5$ are,

$$\rho = 1 \quad (62)$$

$$k = \pi \quad (63)$$

$$Q_0 = 2\pi^2 \quad (64)$$

$$\kappa_{\perp} = 0, \quad (65)$$

$$T(x, y) = \cos(\pi x)\cos(\pi y), \quad (66)$$

$$B_x = \cos(\pi x)\sin(\pi y), \quad (67)$$

$$B_y = -\cos(\pi y)\sin(\pi x). \quad (68)$$

We also choose $T_{bound} = 0$ for the fixed boundary conditions.

Unlike Sharma & Hammett (2007) and Sovinec et al. (2005), our goal here, is to estimate the numerical diffusion in the case of a pure anisotropic conduction ($\kappa_{\perp} = 0$). This numerical diffusion increases with the parallel conductivity with $\kappa_{\perp} = 0$. We obtain κ_{num} by running simulation to steady state and setting $\kappa_{num} = 1/T(0, 0)$. Using this method, we determine the ratio $\kappa_{num}/\kappa_{\parallel}$ as a function of the resolution ($dx/L = 0.01$, $dx/L = 0.02$, $dx/L = 0.05$ and $dx/L = 0.1$) for the different implementations of the conduction. The results are presented on Fig.8.

The first point is that all the methods converge towards lower numerical diffusion with an order of convergence of ≈ 2 (i.e., $\kappa_{num}/\kappa_{\parallel} \propto dx^2$). The least diffusive method is of course the standard asymmetric method. This method reaches a ratio of $\kappa_{num}/\kappa_{\parallel} = 10^{-4}$ for a resolution $dx/L = 0.01$. However, we have already noted in the precedent part that this method could lead to unphysical results and may therefore not be suitable for applications with large

temperature gradients (like in presence of shocks). The method of Sharma & Hammett (2007) circumvents this problem but the perpendicular diffusion is a factor of ≈ 7 more important than in the standard method. On the contrary our new method is only a factor of ≈ 2 more diffusive than the standard method but doesn't lead to negative temperature.

4.2. Conclusion: comparison of the three methods for anisotropic conduction or diffusion

We summarize in Table 1 the properties of the three different methods studied in this section. One of the most important property emphasized by Sharma & Hammett (2007) is to know if the solution remains bounded in the initial range of temperature. Indeed, this is essential to guarantee physical results and stability of the scheme. Unfortunately, the standard asymmetric method doesn't share this property. It still could be used in presence of smooth temperature field taking advantage of its speed (4 times faster than the MHD solver) and accuracy ($\kappa_{num}/\kappa_{\parallel} = 10^{-4}$) but has to be avoided in presence of strong temperature gradient and chaotic magnetic field.

From our knowledge, only two methods for asymmetric conduction (or diffusion) are positive definite. In the first method, an asymmetric discretization is used but the transverse temperature gradients are limited (Sharma & Hammett 2007). This method is almost as fast as the precedent one (three time faster than the MHD solver) but the limiter increases a lot the perpendicular diffusion ($\kappa_{num}/\kappa_{\parallel} = 7 \times 10^{-4}$). The second method, from this article, is based on a physically motivated discretization along the magnetic flux tube. The accuracy then turns out to be better ($\kappa_{num}/\kappa_{\parallel} = 2 \times 10^{-4}$) but it is a little bit slower (although still one time and half faster than the MHD solver). In order to allow the reader to judge which problem size can be realistically treated we give here an indication of the cpu time and the memory consumption for a 3D run with 100^3 grids on an AMD Operon 1.8 GHz. A double time step consisting in two calls to the transport subroutine and two calls to the MHD+cosmic rays routine takes about 30s and uses about 500 MB of memory. We are currently working on a parallel version in order to make larger runs.

Since this method is a non-conservative method, we have also estimated the average fraction of energy lost per time step in the circular conduction test. These losses are limited to about 10^{-5} , which is small considering that the magnetic field is strongly curved and the temperature falls by a factor of 10^4 in few cells. Finally, it is worth noting that even higher level of anisotropy could be reached by implementing a higher order method. This could be easily done by interpolating the temperature field at higher order.

In the present and past section, we have shown that cosmic-ray tests and passive conduction tests were successful. We now move to active conduction tests which involve coupling between the MHD solver, the cosmic-ray solver, as well as the anisotropic transport solver.

5. Buoyancy instabilities

In this section, we focus on buoyancy instabilities in a stratified atmosphere. We present here two applications of our code which serve both as a test of our two-fluid code with anisotropic transport as well as a physical study of the cosmic ray magnetothermal instability (CRMTI).

5.1. Physical background

The cosmic ray magnetothermal instability (CRMTI) (Chandran & Dennis 2006; Dennis & Chandran 2007) is a buoyancy instability that is similar to the Parker instability (Parker 1966; Shu 1974; Ryu et al. 2003) since it involves magnetic fields and cosmic rays. However, in contrast to the Parker instability, the CRMTI involves anisotropic thermal conduction and allows for a temperature gradient in the equilibrium, both of which are relevant for understanding buoyancy instabilities in clusters of galaxies. The CRMTI is very similar to the magnetothermal instability (MTI) (Balbus 2000, 2001; Parrish & Stone 2005, 2007), except that it involves cosmic rays, and, magnetic buoyancy if $\beta = 8\pi p/B^2$ is not large (as in the analysis of Dennis & Chandran (2007)). The stability criterion is given by Dennis & Chandran (2007),

$$nk_B dT/dz + dp_{cr}/dz + de_{mag}/dz > 0, \quad (69)$$

with $e_{mag} = B^2/8\pi$ the magnetic energy density. As discussed by Chandran (2005); Chandran & Raseria (2007), the CRMTI may lead to convection in galaxy cluster cores, since central AGN produce jets and centrally concentrated cosmic rays. Such convection may play an important role in transferring AGN power to the intracluster medium and helping to solve the “cooling flow problem.”

To understand the physics of this instability, let’s take a simple example where this instability applies. Consider a magnetized plasma plus cosmic-ray stratified atmosphere initially at equilibrium with a negligible gradient of magnetic field strength and temperature but a negative gradient of cosmic-ray pressure ($dp_{cr}/dz < 0$). Consider also a vertical gravity along “z” $\mathbf{g} = -g\mathbf{e}_z$ and a horizontal magnetic field along “y”, $\mathbf{B}_0 = B_0\mathbf{e}_y$. If one perturbs this medium by pushing upward a fluid parcel ($\delta v_z > 0$, with δ the difference between the perturbed state in the bubble and the equilibrium state in the surrounding), the magnetic

field lines will be distorted ($\delta B_z \neq 0$). As a consequence of the anisotropic transport, the cosmic ray pressure and plasma temperature will be smoothed along the perturbed field lines, that is to say the temperature and cosmic-ray pressure of the upwardly displaced fluid parcel will be the same as in the initial equilibrium. Therefore, the cosmic ray pressure in the upwardly displaced fluid parcel will be larger than the one of the surrounding medium ($\delta p_{cr} > 0$) and the temperature will be almost the same ($\delta T \approx 0$). Requiring total pressure equilibration with the surrounding medium, it implies that the parcel density is lower than the one of the surrounding medium ($\delta \rho > 0$) to compensate for the high cosmic ray pressure. As a consequence, the parcel moves upward faster, and the medium is convectively unstable. This instability could even be amplified if the temperature gradient is negative since in this case we would have $\delta T > 0$. The latter occurs in the magnetothermal instability (MTI), where $dp_{cr}/dz = 0$ but $dT/dz < 0$ (Balbus 2000).

An important assumption in the above analysis is that $B_{z0} = 0$. If instead $B_{z0} \neq 0$, then there is an equilibrium heat flux in the z direction, which can further contribute to instabilities (Quataert 2008; Parrish & Quataert 2008). However, such “heat-flux buoyancy instabilities” are not considered further in this paper.

The linear analysis for the CRMTI has been done by Chandran & Dennis (2006) and Dennis & Chandran (2007). The dispersion relation is given by

$$\begin{aligned} & \omega^6 - \omega^4 \left[k^2 u^2 + (k^2 + k_y^2) v_A^2 - g \frac{d \ln \rho_0}{dz} \right] \\ & + \omega^2 \left[k^2 k_y^2 v_A^2 (2u^2 + v_A^2) - (k_x^2 + k_y^2) \left(g^2 + (u^2 + v_A^2) g \frac{d \ln \rho_0}{dz} \right) \right] \\ & + k_y^2 v_A^2 \left[-k^2 k_y^2 v_A^2 u^2 + (k_x^2 + k_y^2) \left(g^2 + u^2 g \frac{d \ln \rho_0}{dz} \right) \right] = 0, \end{aligned} \quad (70)$$

with ω the frequency, $\mathbf{k} = (k_x, k_y, k_z)$ the wave vector, $v_A^2 = B_0^2 / (4\pi \rho_0)$ the square of the Alfvén speed and

$$u^2 = \frac{p_0}{\rho_0} \frac{\gamma \omega + i\eta}{\omega + i\eta} + \frac{p_{cr0}}{\rho_0} \frac{\gamma_{cr} \omega}{\omega + i\eta}, \quad (71)$$

$$\nu = k_y^2 D_{\parallel}, \quad (72)$$

$$\eta = k_y^2 D_{\text{cond}}. \quad (73)$$

The eigenfunctions are given by,

$$\delta \rho = -\frac{i \delta v_z}{\omega} \frac{d \rho_0}{dz} + \frac{\mathbf{k} \cdot \delta \mathbf{v} \rho_0}{\omega} \quad (74)$$

$$\delta \mathbf{B} = -\frac{i \delta v_z}{\omega} \frac{d \mathbf{B}_0}{dz} - \frac{k_y B_0 \delta \mathbf{v}}{\omega} + \frac{\mathbf{k} \cdot \delta \mathbf{v} \mathbf{B}_0}{\omega}, \quad (75)$$

$$\delta p = -\frac{i\delta v_z}{\omega} \frac{dp_0}{dz} + \frac{\gamma\omega + i\eta}{\omega + i\eta} \frac{\mathbf{k} \cdot \delta \mathbf{v} p_0}{\omega}, \quad (76)$$

$$\delta p_{cr} = -\frac{i\delta v_z}{\omega} \frac{dp_{cr0}}{dz} + \frac{\mathbf{k} \cdot \delta \mathbf{v} \gamma_{cr} p_{cr0}}{\omega + i\nu}, \quad (77)$$

$$\delta v_x = \frac{H.F - C.E}{A.E - H^2} \delta v_z, \quad (78)$$

$$\delta v_y = \frac{A.F - C.H}{H^2 - A.E} \delta v_z, \quad (79)$$

with $A = -i[\omega^2 - k_y^2 v_A^2 - k_x^2(u^2 + v_A^2)]$, $C = -k_x g + ik_x k_z(u^2 + v_A^2)$, $E = -i(\omega^2 - k_y^2 u^2)$, $F = ik_y k_z u^2 - k_y g$ and $H = ik_x k_y u^2$. For a detailed discussion of this instability see Chandran & Dennis (2006); Dennis & Chandran (2007). Let's now study this instability using our new code.

5.2. An interesting limit: the magnetothermal instability (MTI)

The easiest limit of this system is the adiabatic convective instability (no cosmic ray, no magnetic field, no conduction) which obeys the Schwarzschild stability criterion ($dS/dz > 0$). As a preliminar test we have run a simulation and compared the evolution of the eigenfunction with the analytical one. The agreement between simulation and linear analysis is good. We do not present here the results since it has been abundantly studied in the literature.

A more complex limit arises in dilute plasma when one takes into account anisotropic conduction. Indeed, in this case, the stability criterion becomes $dT/dz > 0$ (Balbus 2000) and the medium could therefore be unstable even if the entropy gradient is positive. Since this instability has already been studied in Parrish & Stone (2005), our main purpose here is to test our code by comparing the numerical solution with the linear analysis. We therefore use a very similar test case to that studied by Parrish & Stone (2005). The main difference is that we trigger only two modes so that we are able to compute the exact linear solution (eigenfunctions).

Our initial conditions for the magnetothermal instability test are therefore a vertical equilibrium state for $-0.05 < y < 0.05$ and $-0.05 < z < 0.05$ (we use here the same axis as in Chandran & Dennis (2006) even if it's a 2D run):

$$\rho(z) = \rho_0 \left(1 - \frac{z}{H_\rho}\right), \quad (80)$$

$$p(z) = p_0 \left(1 - \frac{z}{H_p}\right), \quad (81)$$

$$\mathbf{g} = -\frac{\nabla p_{tot}(z)}{\rho(z)}, \quad (82)$$

$$\mathbf{B} = \sqrt{\frac{8\pi p_0}{\beta}} \mathbf{e}_y, \quad (83)$$

$$(84)$$

with $\rho_0 = p_0 = T_0 = 1$ in appropriate units and $\beta = 2 \times 10^6$ (to be in the high beta limit). By choosing $H_\rho = 1.5$ and $H_p = 1$, as in Parrish & Stone (2005), we ensure that the entropy gradient stays positive but the temperature gradient is negative. The conduction coefficient is $D_{\text{cond}} = 6.8 \times 10^{-5}$. The box length $L = 0.1$ satisfies the condition $L \leq 0.1 \min(H_\rho, H_p)$ which is essential to be able to apply local analysis.

The boundary conditions need to conserve energy and also to not break artificially the initial equilibrium. We therefore choose periodic horizontal boundary conditions and reflective vertical boundary conditions. The implementation of reflective boundary conditions in presence of gravity turns out to be non trivial since the last cells are not in equilibrium if one uses standard reflective boundary conditions. In order to deal with this problem, we assign values to the ghost cells by assuming reflectional symmetry for scalars and reflectional antisymmetry for vectors, including gravity. We also remove the artificial diffusion of the last active cells that is normally added explicitly as part of the TVD method. In this way we could fulfill the two requirements: energy conservation and equilibrium.

We perturb the initial equilibrium with the superposition of two eigenfunctions with same $k_y = 2\pi/L$ but opposite k_z ($k_z = +2\pi/L$ and $k_z = -2\pi/L$) so that the vertical velocity cancels along the horizontal boundaries. We take the amplitude of the velocity perturbation of each mode to be $\delta v_z/c_s = 1.55 \times 10^{-5}$ so that all the perturbed fields stay in the linear regime. Taking such a small value is very important since we will see that the relative amplitude of the magnetic field fluctuations are a factor $\approx c_s k/\sigma \approx 200$ times larger than the one of the velocity. To compute the eigenfunction we take the limit $p_{cr} = 0$ and $D_{\parallel} = 0$ of the eigenfunction of Chandran & Dennis (2006) described in the last subsection. We finally study the most unstable mode which is convective and exponentially growing. For this purpose, we run a 2D simulation with 200 by 200 grid points. The expected growth rate is $\sigma = 0.22$. Note that to obtain the same results as Parrish & Stone (2005) one has to trigger only one eigenfunction with $k_z = 0$ but, in this case, boundary conditions then excite a lot of different and uncontrolled modes.

The results in Fig.9 show good agreement with the analytical result. We however note some slight deformations mainly due to the slope limiter as already mentioned in earlier sections. For example, one could clearly see the clipping of the maxima of δv_z . We have checked that without slope limiters these deformations do not appear. We therefore recover the results of Parrish & Stone (2005), concerning the growth rate. We have presented a test for active anisotropic conduction which turns out to be very strict and give no mercy to any

approximations in any part of the scheme. We have noticed that a simple precision run or a too violent slope limiter quickly destroy the shape of the sines.

5.3. Solution of the full system: the cosmic-ray magnetothermal instability (CRMTI)

This code is especially dedicated to the study of this instability. This part serves as a cross-validation between our code and the analytical predictions of Chandran & Dennis (2006). We use here the same kind of initial condition as in the study of the magnetothermal instability. The difference is that we have now cosmic rays and we therefore take,

$$p_{cr}(z) = p_{cr0} \left(1 - \frac{z}{H_{cr}}\right). \quad (85)$$

$$(86)$$

Instead of choosing the same density and pressure gradients for the plasma as Parrish & Stone (2005), we prefer to study a different situation where the gradient of entropy and the gradient of temperature are positive. In this case, both the Schwarzschild stability criterion and the Balbus (2000) stability criterion are satisfied. However, we choose a negative gradient of cosmic rays so that the atmosphere is convectively unstable according to Eq.69. This kind of situation is expected in the center of cluster of galaxies (Chandran 2005; Chandran & Dennis 2006; Dennis & Chandran 2007; Chandran & Rasera 2007; Rasera & Chandran 2008). Since we are mainly interested in the role of cosmic rays, we take a nul gradient of magnetic field so that the magnetic field doesn't modify the stability criterion (Dennis & Chandran 2007).

Our initial conditions are inspired by the Perseus cluster at 50 kpc (Chandran & Dennis 2006). Namely, we take $T_0 = 4$ keV, an electronic density $n_{e0} = 0.02 \text{ cm}^{-3}$, an ion density of $n_{i0} = 0.9n_e$, a mean molecular weigh of $\mu = 0.6$, a cosmic ray pressure $p_{cr0} = p_0$ and a magnetic field of $B_0 = 1 \text{ } \mu\text{G}$. For these values, the conduction coefficient is $D_{\text{cond}} = 2.5 \times 10^{30} \text{ cm}^2/\text{s}$ and we choose the diffusion coefficient to be $D_{\parallel} = 10^{29} \text{ cm}^2.\text{s}^{-1}$ (see Sect.2). Concerning the gradient, we take a negative density gradient with $H_\rho = 50$ kpc, a positive temperature gradient with $H_T = 200$ kpc, and a negative cosmic ray gradient with $H_{cr} = 50$ kpc. We finally use 100 by 100 grid points for a simulation box length of $L = 10$ kpc. The amplitude of our two perturbations is $\delta v_z/c_s = 1.44 \times 10^{-5}$ and their wavelength is 10 kpc. We use the same boundary conditions as before and the expected growth rate is $\sigma = 9.5 \times 10^{-3} \text{ Myr}^{-1}$.

Here again the results show good agreement with the linear theory (Fig.10). The extrema of velocity are affected by the limiter. Little numerical errors appear on the temperature fluctuations because they have the smallest relative amplitude and are therefore the

most sensitive to numerical approximations (such as the one induced by the slope limiter). The cosmic-ray pressure is computed with the same accuracy as the plasma pressure. This validates our overall implementation.

On the physical point of view, this simulation illustrates the scenario presented in part 5.1. The phase of δB_z is shifted from $\approx \pi/2$ compared to the phase of δv_z , since the field lines are distorted. The fluctuations of temperature δT are very small. The perturbation δp_{cr} is roughly in phase with δv_z and is amplified, which in turn amplifies δv_z . Even though the entropy and temperature gradients are positive (and the magnetic field energy gradient is nul), the convective instability is growing on a timescale of 10^8 yr which is of order of the cooling time near the center of cooling-flow clusters. This suggests that cosmic rays and anisotropic transport might play an important role in cluster of galaxies.

6. Conclusion

This article could be viewed as a test guide for those who want to implement cosmic-ray and anisotropic transport routines, which are essential ingredients to simulate cooling-flow clusters. We indeed used many linear and non-linear tests for each physical ingredient as well as a new linear test for the full system. Our contribution could be divided into three parts.

First, we showed that the TVD method of Pen et al. (2003) can be used to evolve the cosmic rays and the plasma simultaneously. The shock tube problem for a composite of plasma and cosmic rays is an example of the successful implementation. Second, we insisted on the importance of having a positive implementation of the anisotropic conduction in order to ensure physical results even in the presence of sharp gradients. We therefore presented a new flux-tube method which has two important properties: positivity and accuracy. This is important for clusters of galaxies since the conduction is highly anisotropic as opposed to a very diffusive scheme. Moreover, the random magnetic fields and potential large temperature and cosmic-ray-pressure gradients in cluster cores may cause negative temperatures in a non-positive scheme. Third, the linear regime of the cosmic ray magnetothermal instability (CRMTI) provides a new, sensitive test, of the overall implementation. The main interest is that this instability has a broader range of applications since the criterion is $nk_B dT/dz + dp_{cr}/dz + de_{mag}/dz > 0$. One interesting future application of this code concerns the cores of clusters of galaxies. Indeed, in these regions, negative radial gradients of cosmic-ray pressure may trigger convection. Moreover, possible large gradients of cosmic-ray pressure near the edges of X-ray cavities (cosmic-ray bubbles) require positive implementation of the anisotropic transport. It is worth noting that even though our discussion has focused

mainly on clusters of galaxies, the flux-tube method that we have developed could be used to simulate a variety of physical systems, including the interstellar medium, fusion plasmas, and supernovae-remnants.

We are grateful to U.-L. Pen, T. Dennis, P. Sharma, W. Hammett, R. Teyssier, I. Parrish and J. Stone for their valuable comments and suggestions.

REFERENCES

- Balbus, S. A. 2000, *ApJ*, 534, 420
- Balbus, S. A. 2001, *ApJ*, 562, 909
- Balsara, D. S., Tilley, D. A., & Howk, J. C. 2008, *MNRAS*, 386, 627
- Bîrzan, L., Rafferty, D. A., McNamara, B. R., Wise, M. W., & Nulsen, P. E. J. 2004, *ApJ*, 607, 800
- Boehringer, H., & Morfill, G. E. 1988, *ApJ*, 330, 609
- Boehringer, H., Matsushita, K., Churazov, E., & Finoguenov, A. 2004, *The Riddle of Cooling Flows in Galaxies and Clusters of galaxies*, 189
- Braginskii, S. I. 1965, *Reviews of Plasma Physics*, vol. 1, ed. M.A. Leontovitch, 205
- Brighenti, F., & Mathews, W. G. 2006, *ApJ*, 643, 120
- Brüggen, M., Kaiser, C. R., Churazov, E., & Enßlin, T. A. 2002, *MNRAS*, 331, 545
- Brüggen, M., & Kaiser, C. R. 2002, *Nature*, 418, 301
- Brüggen, M., Ruszkowski, M., & Hallman, E. 2005, *ApJ*, 630, 740
- Cattaneo, A., & Teyssier, R. 2006, *ArXiv Astrophysics e-prints*, arXiv:astro-ph/0611914
- Chandran, B. D. G., & Cowley, S. C. 1998, *Physical Review Letters*, 80, 3077
- Chandran, B. D. G. 2001, *Space Science Reviews*, 99, 271
- Chandran, B. D. G. 2004, *ApJ*, 616, 169
- Chandran, B. D. G., & Maron, J. L. 2004, *ApJ*, 602, 170

- Chandran, B. D. G. 2005, *ApJ*, 632, 809
- Chandran, B. D., & Dennis, T. J. 2006, *ApJ*, 642, 140
- Chandran, B. D., & Rasera, Y. 2007, *ApJ*, 671, 1413
- Churazov, E., Forman, W., Jones, C., Böhringer, H. 2000, *A&A*, 356, 788
- Churazov, E., Brüggén, M., Kaiser, C. R., Böhringer, H., & Forman, W. 2001, *ApJ*, 554, 261
- Churazov, E., Forman, W., Jones, C., Sunyaev, R., Böhringer, H. 2004, *MNRAS*, 347, 29
- Cole, S., Lacey, C. G., Baugh, C. M., & Frenk, C. S. 2000, *MNRAS*, 319, 168
- Dennis, T. J. & Chandran, B. D. 2008, *ApJ*, submitted
- Drury, L. O., & Voelk, J. H. 1981, *ApJ*, 248, 344
- Dunn, R. J. H., & Fabian, A. C. 2006, *MNRAS*, 373, 959
- Eilek, J. A. 2004, *The Riddle of Cooling Flows in Galaxies and Clusters of galaxies*, 165
- Enßlin, T. A., Vogt, C., & Pfrommer, C. 2004, *The Riddle of Cooling Flows in Galaxies and Clusters of galaxies*, 145
- Fabian, A. C., Nulsen, P. E. J., & Canizares, C. R. 1991, *A&A Rev.*, 2, 191
- Fabian, A. C., Voigt, L. M., & Morris, R. G. 2002, *MNRAS*, 335, L71
- Fabian, A. C., Sanders, J. S., Allen, S. W., Crawford, C. S., Iwasawa, K., Johnstone, R. M., Schmidt, R. W., & Taylor, G. B. 2003, *MNRAS*, 344, L43
- Fabian, A. C., Sanders, J. S., Crawford, C. S., Conselice, C. J., Gallagher, J. S., & Wyse, R. F. G. 2003, *MNRAS*, 344, L48
- Fabian, A. C. 2005, *Royal Society of London Philosophical Transactions Series A*, 363, 725
- Forman, W., et al. 2005, *ApJ*, 635, 894
- Gould, R. J. 1972, *Physica*, 58, 379
- Guo, F., Oh, S. P., & Ruszkowski, M. 2008 arXiv:0804.3823
- Hatton, S., Devriendt, J. E. G., Ninin, S., Bouchet, F. R., Guiderdoni, B., & Vibert, D. 2003, *MNRAS*, 343, 75

- Hawley, J. F., Wilson, J. R., & Smarr, L. L. 1984, *ApJ*, 277, 296
- Heinz, S., Brügggen, M., Young, A., & Levesque, E. 2006, *MNRAS*, 373, L65
- Jones, T. W., & Kang, H. 1990, *ApJ*, 363, 499
- Jones, T. W., & Kang, H. 2005, *Astroparticle Physics*, 24, 75
- Jubelgas, M., Springel, V., & Dolag, K. 2004, *MNRAS*, 351, 423
- Jubelgas, M., Springel, V., Enlin, T., & Pfrommer, C. 2008, *A&A*, 481, 33
- Kauffmann, G., Colberg, J. M., Diaferio, A., & White, S. D. M. 1999, *MNRAS*, 303, 188
- Kronberg, P. P. 1994, *Nature*, 370, 179
- Loewenstein, M., & Fabian, A. C. 1990, *MNRAS*, 242, 120
- Loewenstein, M., Zweibel, E. G., & Begelman, M. C. 1991, *ApJ*, 377, 392
- Maron, J., Chandran, B. D., & Blackman, E. 2004, *Physical Review Letters*, 92, 045001
- Mathews, W. G., Brighenti, F., Buote, D. A., & Lewis, A. D. 2003, *ApJ*, 596, 159
- Mathews, W., & Brighenti, F. 2008, arXiv:0805.2441
- McNamara, B. R. 2004, *The Riddle of Cooling Flows in Galaxies and Clusters of galaxies*, 177
- Miniati, F. 2001, *Comp. Phys. Comm.*, 141 17
- Miniati, F. Jones, T. W., Kang, H., & Ryu, D. 2001, *ApJ*, 562, 233
- Narayan, R., & Medvedev, M. V. 2001, *ApJ*, 562, L129
- Nulsen, P. 2004, *The Riddle of Cooling Flows in Galaxies and Clusters of galaxies*, 259
- Omma, H., & Binney, J. 2004, *MNRAS*, 350, L13
- Omma, H., Binney, J., Bryan, G., & Slyz, A. 2004, *MNRAS*, 348, 1105
- Parker, E. N. 1958, *ApJ*, 128, 664
- Parker, E. N. 1966, *ApJ*, 145, 811
- Parrish, I. J., & Stone, J. M. 2005, *ApJ*, 633, 334

- Parrish, I. J., & Stone, J. M. 2007, ApJ, submitted
- Parrish, I. J., & Quataert, E. 2008, ApJL, 677, 9
- Pen, U.-L. 1998, ApJS, 115, 19
- Pen, U.-L., Arras, P., & Wong, S. 2003, ApJS, 149, 447
- Peterson, J. R., Kahn, S. M., Paerels, F. B. S., Kaastra, J. S., Tamura, T., Bleeker, J. A. M., Ferrigno, C., & Jernigan, J. G. 2003, ApJ, 590, 207
- Pfrommer, C., Springel, V., Enßlin, T. A., & Jubelgas, M. 2006, MNRAS, 367, 113
- Quataert, E. 2008, ApJ, 673, 758
- Quilis, V., Bower, R. G., & Balogh, M. L. 2001, MNRAS, 328, 1091
- Rasera, Y., & Teyssier, R. 2006, A&A, 445, 1
- Rasera, Y., & Chandran, B. 2008, ApJ, submitted
- Rechester, A. B., & Rosenbluth, M. N. 1978, Physical Review Letters, 40, 38
- Reynolds, C. S., Heinz, S., & Begelman, M. C. 2001, ApJ, 549, L179
- Reynolds, C. S., Heinz, S., & Begelman, M. C. 2002, MNRAS, 332, 271
- Reynolds, C. S., McKernan, B., Fabian, A. C., Stone, J. M., & Vernaleo, J. C. 2005, MNRAS, 357, 242
- Ruszkowski, M., & Begelman, M. C. 2002, ApJ, 581, 223
- Ruszkowski, M., Brüggén, M., & Begelman, M. C. 2004, ApJ, 611, 158
- Ruszkowski, M., Brüggén, M., & Begelman, M. C. 2004, ApJ, 615, 675
- Rosner, R., & Tucker, W. H. 1989, ApJ, 338, 761
- Ryu, D., Kim, J., Hong, S. S., & Jones, T. W. 2003, ApJ, 589, 338
- Sijacki, D., & Springel, V. 2006, MNRAS, 371, 1025
- Sharma, P., & Hammett, G. W. 2007, Journal of Computational Physics, 227, 123
- Shu, F. H. 1974, A&A, 33, 55
- J. Skilling, Monthly Notices Roy. Astron. Soc. 172 (1975) 557.

- Somerville, R. S., & Primack, J. R. 1999, MNRAS, 310, 1087
- Sod, G. A. 1978, J. Comput. Phys., 27, 1
- Soker, N., & Pizzolato, F. 2005, ApJ, 622, 847
- Sovinec C. R., & NIMROD Team. 2005, J. Comp. Phys., 195, 355
- Spitzer, L. 1962, Physics of Fully Ionized Gases, New York: Interscience (2nd edition), 1962
- Springel, V., & Hernquist, L. 2003, MNRAS, 339, 312
- Taylor, G. B., Govoni, F., Allen, S. W., & Fabian, A. C. 2001, MNRAS, 326, 2
- Taylor, G. B., Fabian, A. C., & Allen, S. W. 2002, MNRAS, 334, 769
- Trac, H., & Pen, U.-L. 2003, PASP, 115, 303
- Vernaleo, J. C., & Reynolds, C. S. 2006, ApJ, 645, 83
- Vogt, C., & Enßlin, T. A. 2003, A&A, 412, 373
- Voigt, L. M., Schmidt, R. W., Fabian, A. C., Allen, S. W., & Johnstone, R. M. 2002, MNRAS, 335, L7
- Zakamska, N. L., & Narayan, R. 2003, ApJ, 582, 162

Method	positive	diffusion	speed2D	speed3D	losses
standard	NO	10^{-4}	4.2	4.6	10^{-10}
limited	YES	7×10^{-4}	3.3	3.8	10^{-10}
flux tube	YES	2×10^{-4}	1.6	1.0	10^{-5}

Table 1: Summary of the three second order methods for anisotropic conduction or diffusion.

Note. — Columns indicate respectively: the method (standard asymmetric discretization, Van Leer limited or flux tube method), the positivity of the solution, the value of $\kappa_{num}/\kappa_{\parallel}$ in the Sovinec test, the speed relative to the MHD solver in 2D and 3D CRMTI instability test (see Sect.5.3) and the fraction of energy lost per time step at the end of the circular conduction test.

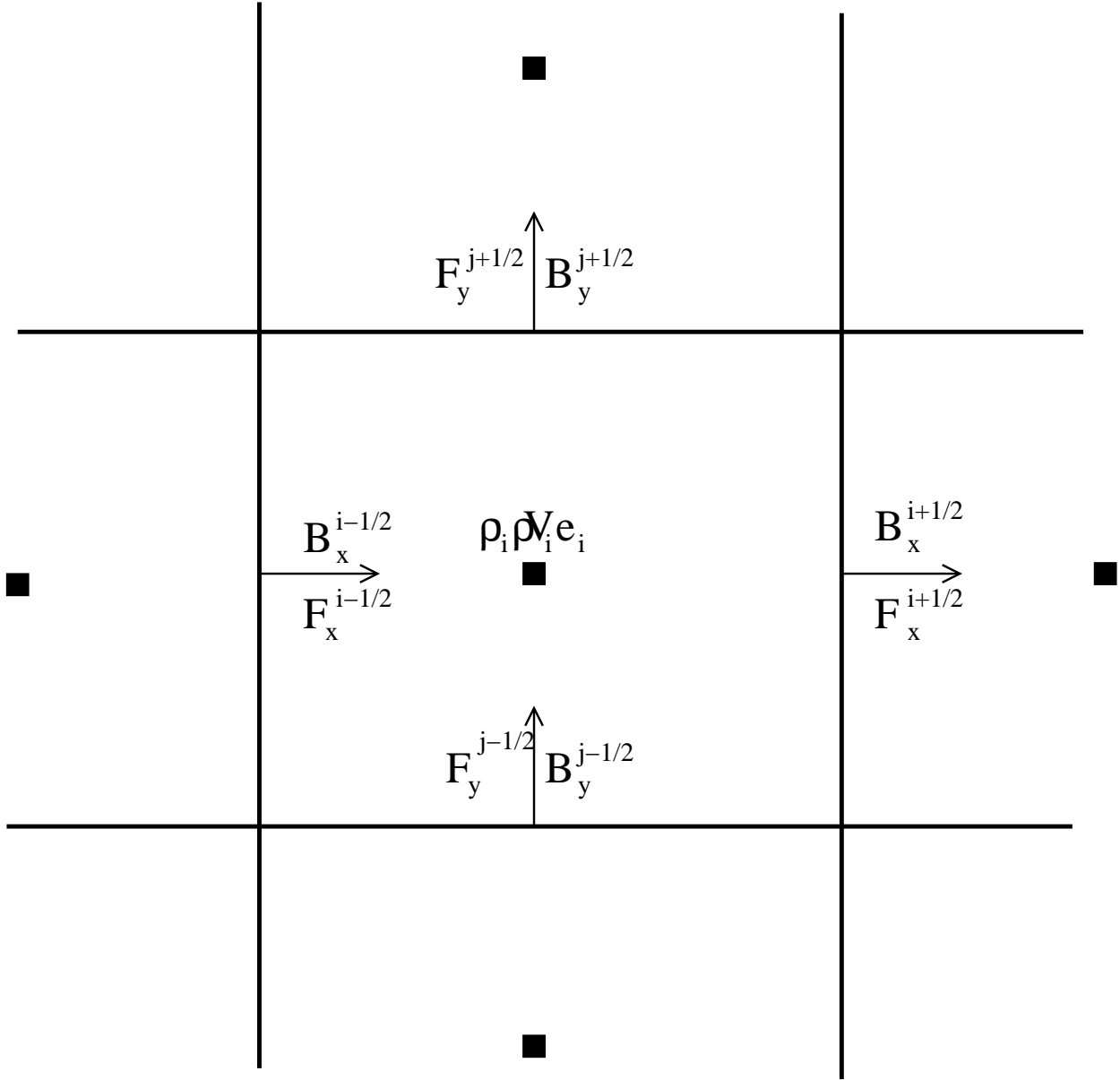


Fig. 1.— Staggered grid used by the MHD solver. Density, momentum and energy are defined at the cell center whereas magnetic fields are defined on the faces. Fluxes are also computed on the faces and depend on the neighbours (squares).

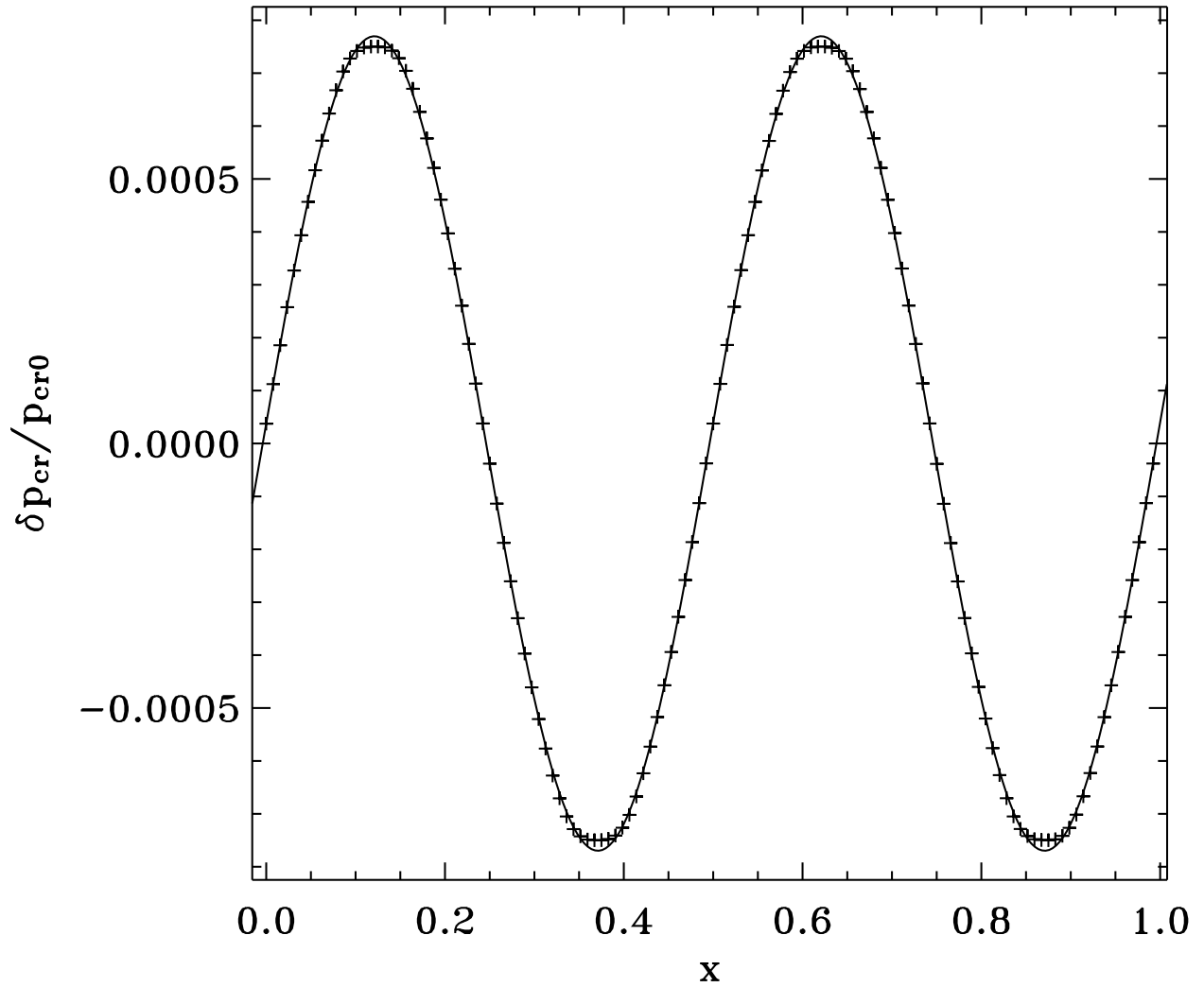


Fig. 2.— Sound wave in a composite of cosmic rays and thermal gas propagated for one wave period. Plus signs represent the simulation cosmic-ray internal energy for 128 grid points whereas the continuous line is the analytical solution.

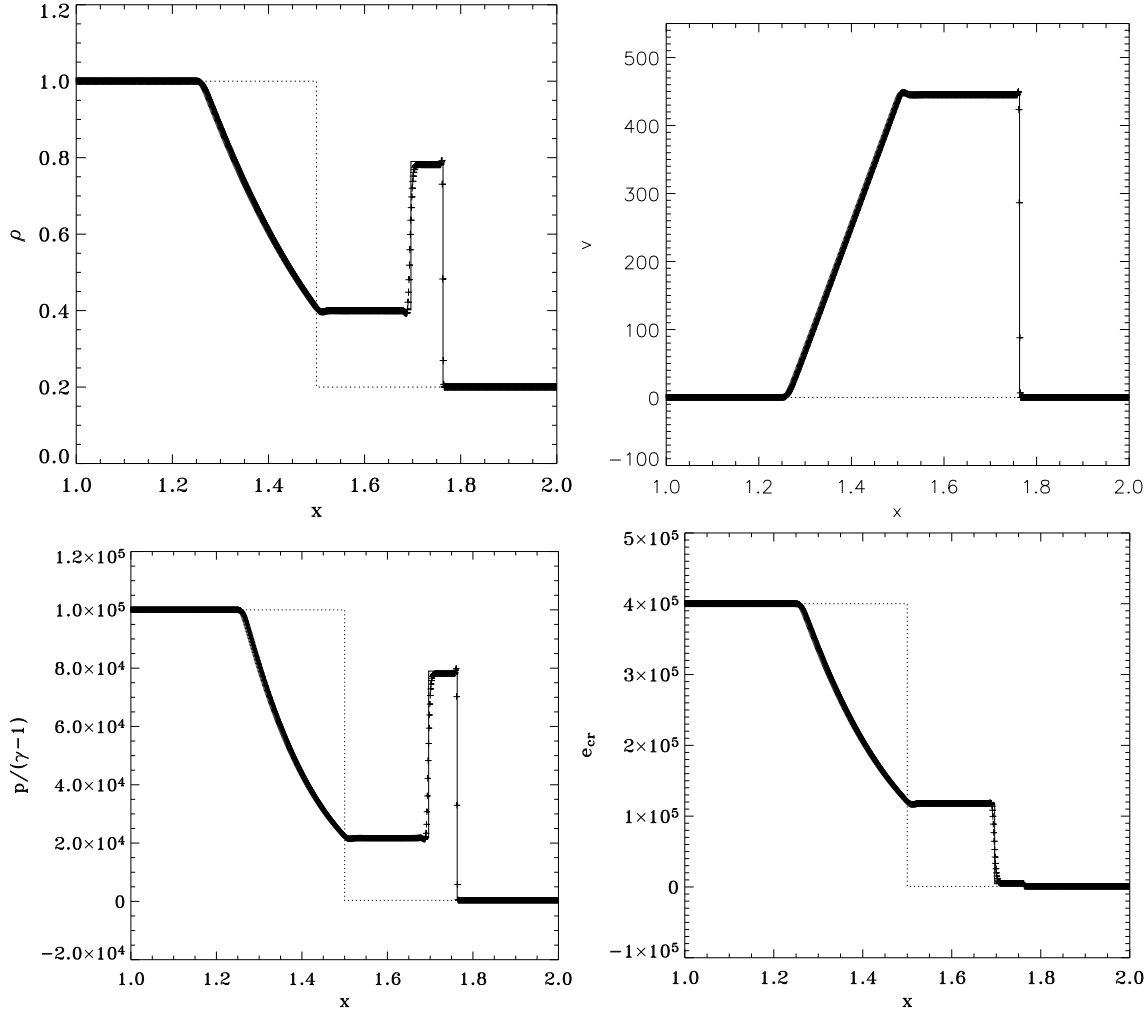


Fig. 3.— Shock tube problem for a composite of cosmic rays and thermal gas. Plus signs show results for a 1024 grid points simulation whereas the continuous line is the analytical solution. The dotted line is the initial condition. The first graph shows the density profile, the second one the velocity profile, the third one the gas internal energy profile and finally the fourth one shows the cosmic-ray internal energy.

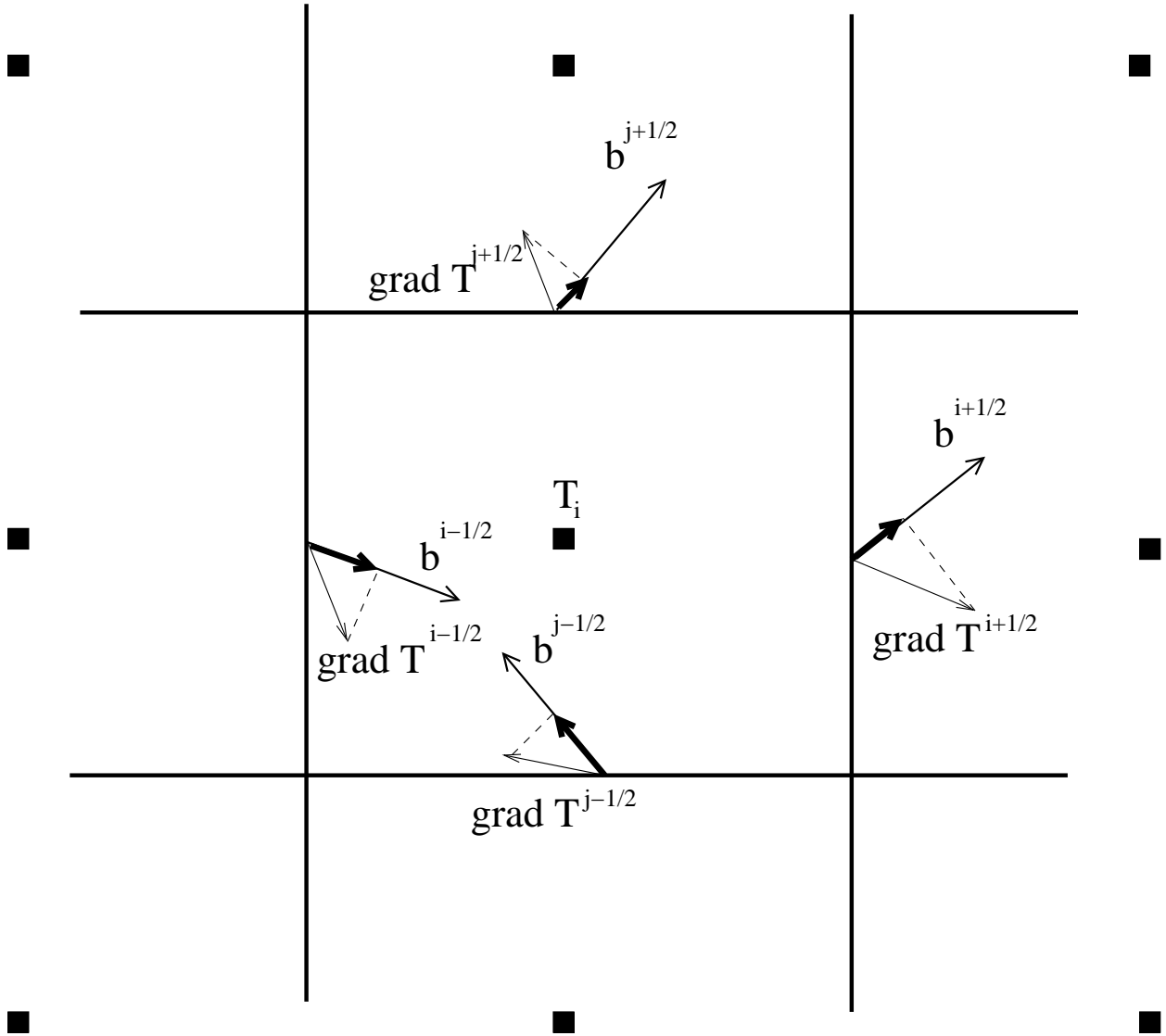


Fig. 4.— In the centered asymmetric method, the heat fluxes on each faces (bold arrows) are computed by projecting temperature gradients on the magnetic field. Temperature gradients computation require the knowledge of the neighbours (squares).

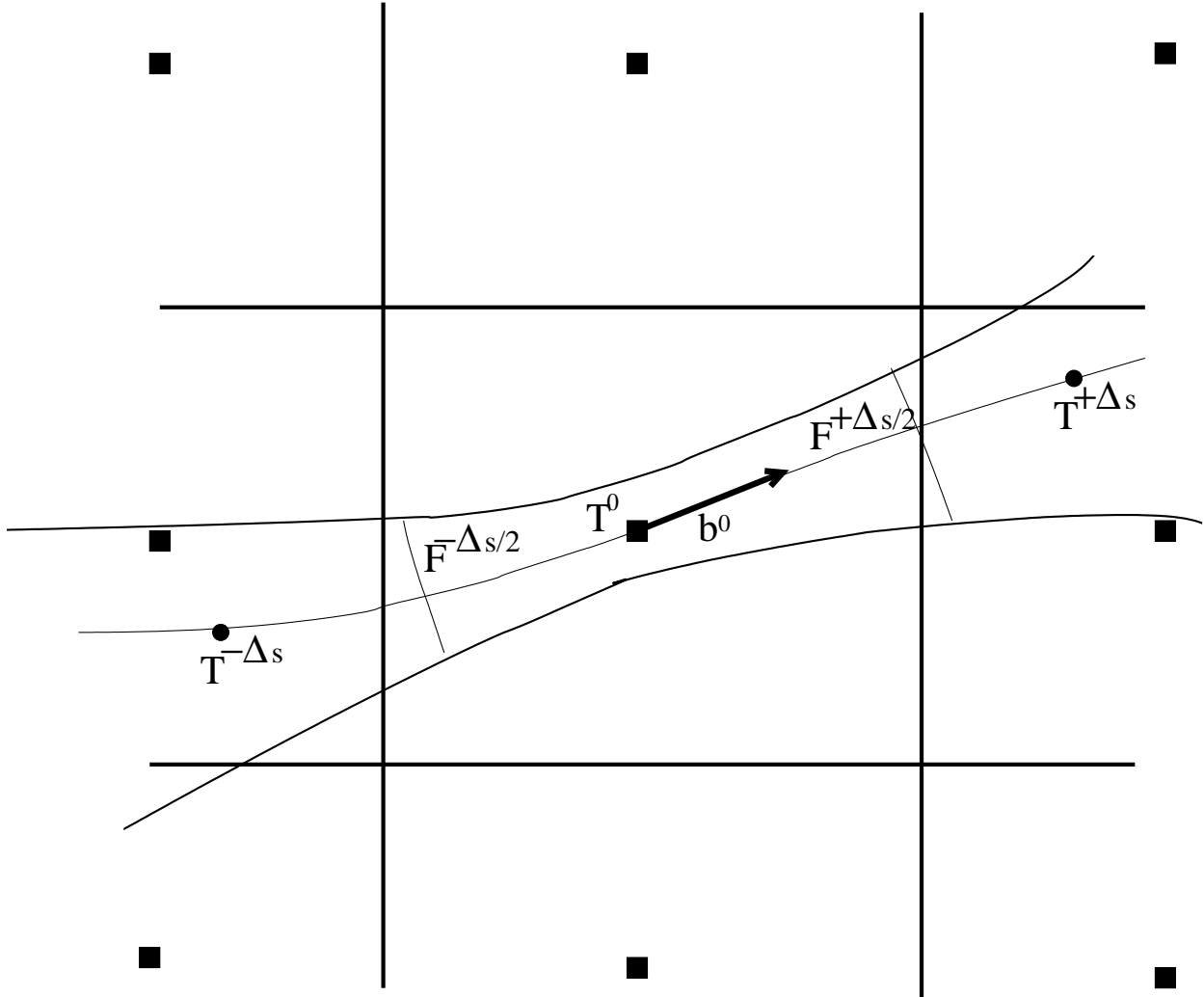


Fig. 5.— In the flux-tube method, one considers a thin magnetic flux tube around T_0 . The evolution of this temperature depends on the heat flux along the magnetic field which is evaluated on the two faces at a distance $\Delta s/2$ from the center: $F^{\pm \Delta s/2}$. These fluxes are deduced from the temperatures $T^{\pm \Delta s}$ which are themselves computed using all the neighbours (squares).

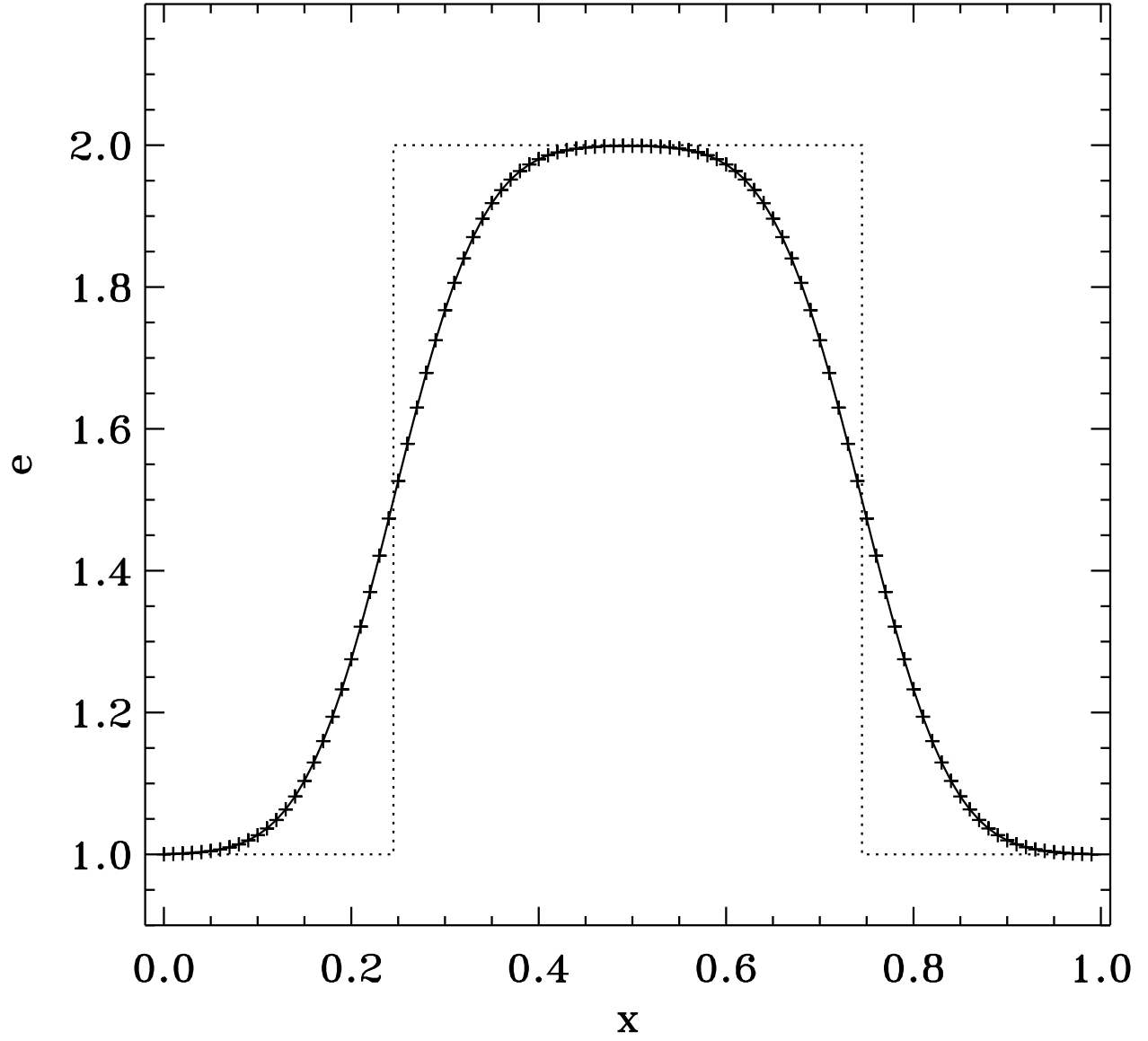


Fig. 6.— Diffusion of 2 1D Heaviside functions (dotted line). The simulation points (plus signs) match well with the analytical result (line).

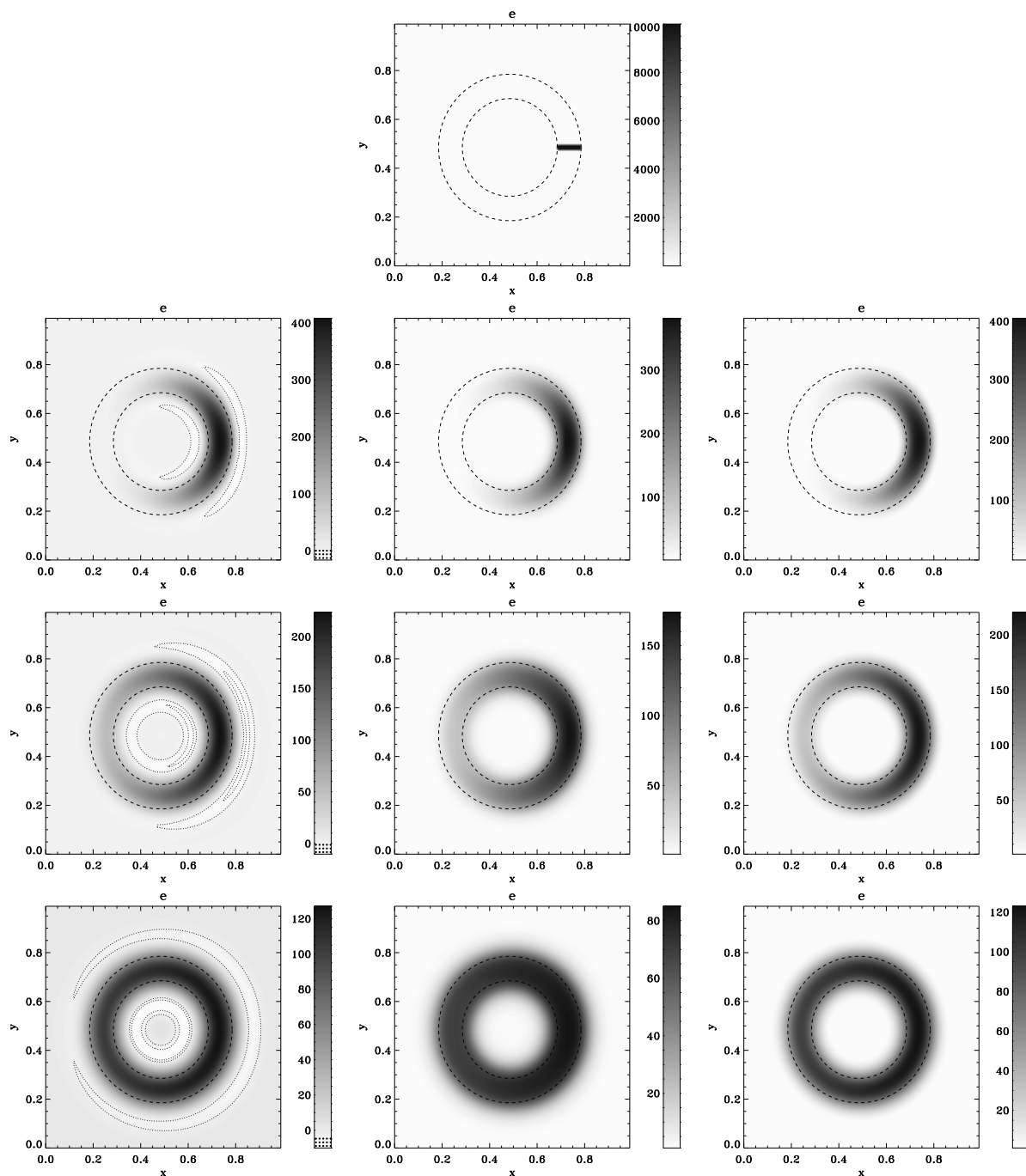


Fig. 7.— Anisotropic diffusion of a hot patch (first graph from the top) along circular magnetic field in a simulation with 100^2 grid points. Columns correspond respectively to, the standard centered asymmetric discretization, the Van-Leer limited methods and our new flux-tube method. Lines correspond respectively to $t = 0.0225$, $t = 0.0675$ and $t = 0.18$. The circles are the field lines confining the heat. Note the negative temperature (dotted contours) in the first method and the considerable perpendicular diffusion in the second method.

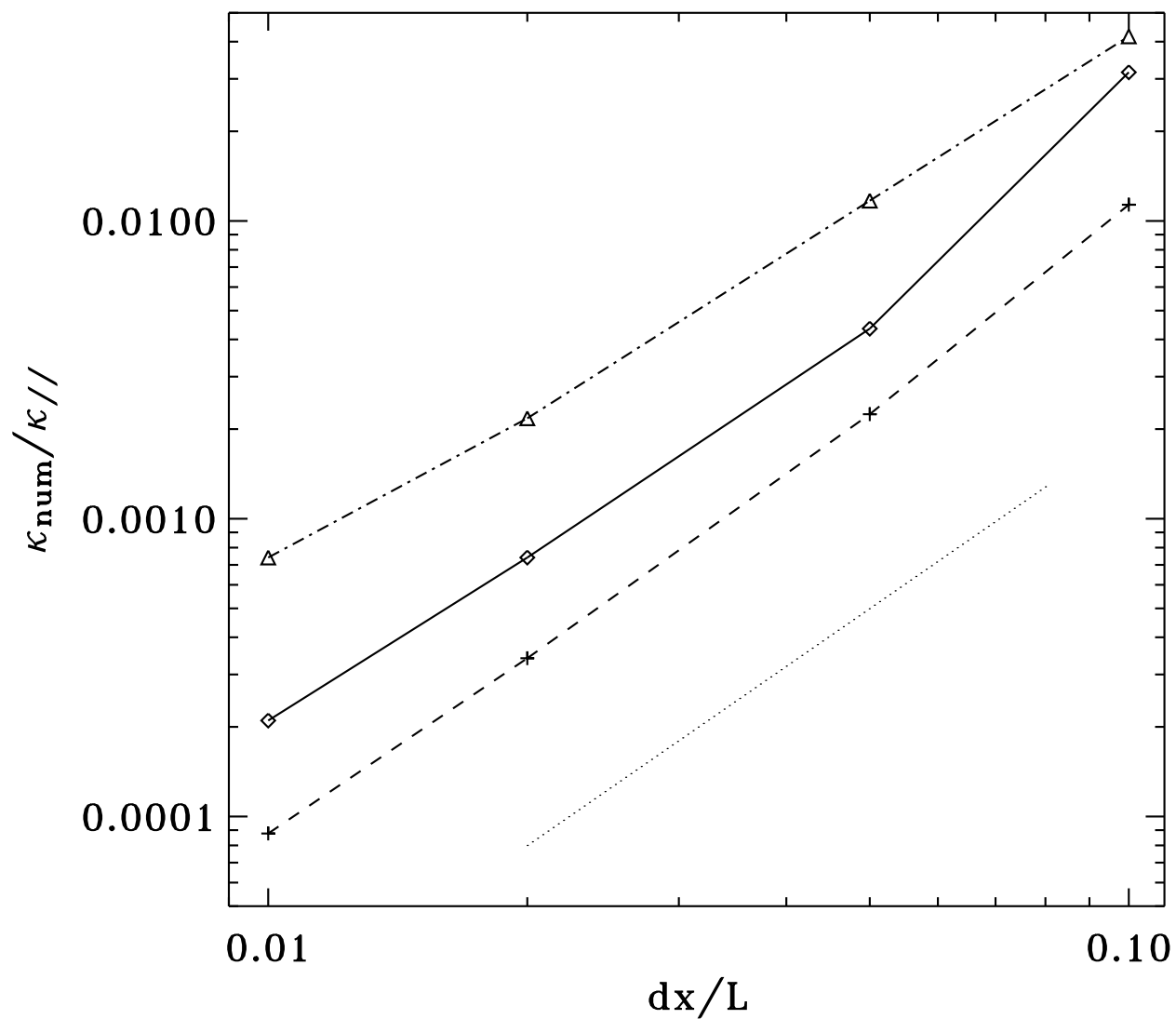


Fig. 8.— Measure of the perpendicular numerical diffusion $\kappa_{\text{num}}/\kappa_{\parallel}$ in the Sovinec et al. (2005) test as a function of the resolution. The dashed curve is the result for the standard asymmetric discretization. The dash-dotted curve is for the Van-Leer-limited method from Sharma & Hammett (2007). Finally, the continuous curve is for our new flux-tube method. For reference, the dotted line has a slope of 2.

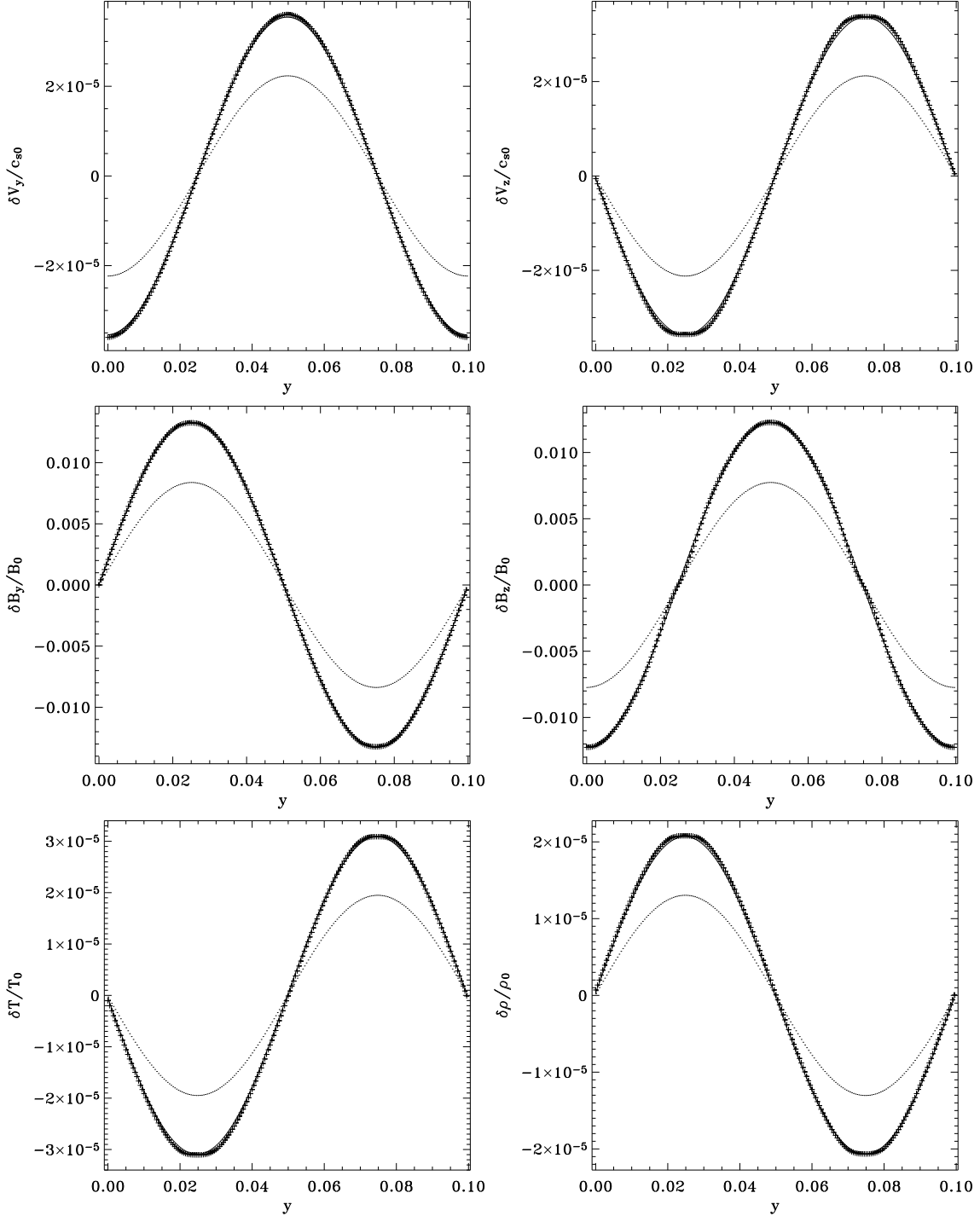


Fig. 9.— Evolution of the eigenfunction in the code (plus signs) compared to the linear theory (solid line). The initial condition is the dotted line. The 6 graphs represent a slice in $z = 0.0125$ for respectively $\delta v_y / c_s$, $\delta v_z / c_s$, $\delta B_y / B_0$, $\delta B_z / B_0$, $\delta T / T_0$ and $\delta \rho / \rho_0$.

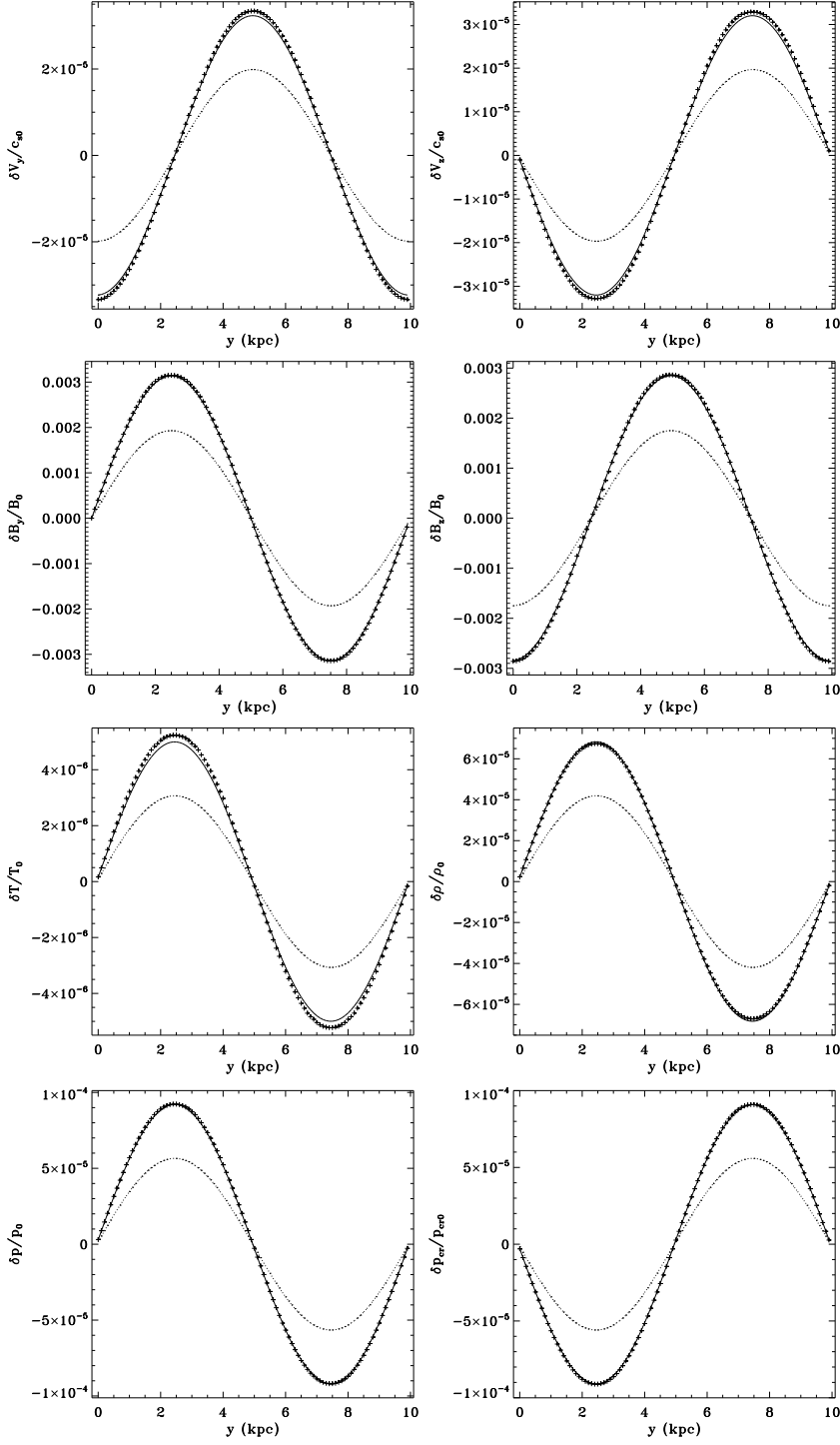


Fig. 10.— Evolution of the eigenfunction in the code (plus signs) compared to the linear theory (solid line, in most case covered by the plus signs). The initial condition is the dotted line. The 6 graphs represent a slice in $z = 6.2$ kpc for respectively, $\delta v_y/c_s$, $\delta v_z/c_s$, $\delta B_y/B_0$, $\delta B_z/B_0$, $\delta T/T_0$, $\delta \rho/\rho_0$, $\delta p/p_0$ and $\delta p_{cr}/p_{cr0}$.